EVIDENCE FOR GROUND MOTION POLARIZATION ON FAULT ZONES OF MT. ETNA VOLCANO

Rosaria Rigano[1], Fabrizio Cara[2], Giuseppe Lombardo[1], and Antonio Rovelli[2]

[1] Dipartimento di Scienze Geologiche, Università di Catania, Catania, Italy

[2] Istituto Nazionale di Geofisica e Vulcanologia, Roma, Italy

Abstract

During local and regional earthquakes, an evident amplification of horizontal ground motion is observed at two seismological stations near the Tremestieri fault, on the southeastern flank of Mt. Etna volcano. Rotated-component spectral ratios show a narrow spectral peak around 4-Hz along a N40°E direction. A conventional polarization analysis using the eigenvectors of the covariance matrix confirms the very stable directional effect enhancing the approximately NE-SW elongation of the horizontal ground motion in the fault zone. The effect is evident during the entire seismogram and independent of source backazimuth as well as distance and depth of earthquakes. The same polarization is observed in ambient noise as well. This consistency allowed us to use microtremors for checking ground motion polarization along and across the Tremestieri fault zone with a high spatial resolution. The result is a stable polarization of horizontal motion in the entire area, interesting a broad frequency band. To check whether this ground motion property is recurrent and understand a possible relationship with fault strike, faulting style, or orientation of

fractures, ambient noise was recorded on other mapped faults of the Mt. Etna area, the Moscarello, Acicatena and Pernicana faults. The latter, in particular, is characterized by different strike and faulting style. A systematic tendency of ambient noise to be polarized is found in all of the faults. A picture emerges where normal faults of the eastern flank show a E-W to NE-SW polarization that changes on the Pernicana fault, which develops approximately E-W and is characterized by a prevailing NW-SE to N-S polarization.

Directions of polarization were never parallel to the fault strike. Moreover, polarization persists too far away from the fault trace, excluding an effect limited to a narrow low velocity zone hosted between harder wall rocks. Both these observations rule out an interpretation in terms of fault-trapped waves. The cause of observed polarizations will be the subject of future studies. However, the consistency with recent results of velocity anisotropy in a part of the investigated area suggests a possible role of attenuation anisotropy on horizontal amplitude variations versus azimuth.

1. Introduction

On September 1998 till August 2002, researchers of Istituto Nazionale di Geofisica e Vulcanologia (INGV) of Rome and Department of Geological Science of the Catania University instrumented 10 sites in the city of Catania to study local effects for microzoning purposes. Two seismological stations were deployed in the Tremestieri fault area to investigate possible effects of fractured lava on ground motion. In general, the highly fractured low-velocity zone bounded by higher-velocity intact rock is known to behave as a wave guide where incident seismic energy is trapped causing a local amplification in the fault zone. The amplification of ground motion tends to be maximum along the fault-parallel direction. There is a large number of papers that describe propagation properties of fault-guided waves both in a theoretical approach [*Ben-Zion and Aki*, 1990; *Li and Vidale*, 1996; *Igel et al.*, 2002; *Jahnke et al.*, 2002] and through observations [*Li et al.*, 1990, 1994 and 2000], mostly in California. There are also study cases of fault-guided waves in Turkey and Italy. On the North Anatolian fault, *Ben Zion et al*. [2003] observed fault-guided waves showing a constant arrival delay from S waves for different epicentral distances. They interpreted this observation as an evidence of a trapping mechanism limited to the uppermost 3-5 kms of that fault zone. A similar conclusion was reached by *Lewis et al*. [2005] who analyzed the seismograms of hundreds small earthquakes recorded across the San Jacinto fault near Anza, California. They also observed a predominance of fault-parallel motion in the fault zone. *Rovelli et al*. [2002] used the fault-guided waveforms of a vertically incident subcrustal earthquake to constrain depth and velocity contrast of the Nocera Umbra fault zone. Also for this fault the conclusion was that polarization of horizontal motion was parallel to the fault strike and the trapping portion of that fault was shallow (1-1.5 km). For the same fault, *Cultrera et al*.

[2003] observed that hodograms of the 0.6 g pulse recorded during the M_L 5.6 and 5.8 earthquakes of September 26, 1997 were consistent with the local fault orientation in distinct contrast with the source mechanism of those earthquakes. In California, *Boore et al*. [2004] observed a similar discrepancy at an accelerographic station in the Calaveras fault zone that recorded the 1984, Morgan Hill earthquake: the largest motion was parallel to the fault and not perpendicular as expected along the fault for a strike-slip mechanism. The same polarization, contradicting the focal mechanism expectation, was observed at that station also during the 1979 Loma Prieta earthquake whose rupture fault plane was approximately parallel to the Calaveras fault, a ten kilometers to the southwest.

In this paper, we first analyze the waveforms of 131 earthquakes recorded at two seismological stations installed near the Tremestieri fault. Ground motion amplitudes are compared with those recorded at a reference station installed on massive lavas in downtown Catania. The evidence of a significant directional amplification during earthquakes and the finding of a similar horizontal polarization in the ambient noise records, motivated an investigation with high spatial resolution measuring microtremors, extending the study to other faults of Mt. Etna. For all of them, the result was that ambient noise as well as earthquake-induced ground motions are strongly polarized along azimuths that vary from zone to zone. However, the model of fault-guided waves does not fit these observations. Alternative interpretations (e.g. near-surface anisotropy) are tentatively tested, however need further seismological data including new experiments in the field as well as laboratory tests on lava samples.

2. Local geology and structural setting

Tectonics of Mt. Etna is the result of the interaction between the regional tectonics and local scale volcano-related processes [*McGuire and Pullen*, 1989]. The western flank of the volcano is interested by a modest tectonic activity, the Ragalna and Calcerana faults [*Azzaro*, 1999] being the main structures (Figure 1a). Conversely, the eastern flank of the volcano is crossed by several youngest NNW- and NNE-trending fault segments causing a sharp morphology in the topography and showing steep escarpments [*Monaco et al.*, 1997]. Most of the faults affecting the eastern flank are highly seismogenic and generate shallow earthquakes as well as coseismic cracks in the soil and creep phenomena [*Azzaro et al.*, 1998; *Azzaro*, 1999; *Azzaro et al.*, 2000]. This system, locally called "Timpe" (Figure 1a), represents the northernmost prolongation of the Malta Escarpment (Figure 1b) and forms a NNW-SSE-trending system of parallel step-faults of considerable length (8-10 Km) having vertical offsets up to 200 m that down-throw towards the sea. Among such structures, the NW-SE trending Tremestieri fault shows a distinct morphological evidence (Figure 1a). To the north, the Timpe system to which also belongs the Moscarello fault, is stopped by the approximately E-W trending Pernicana fault which cuts a large part of the volcanic edifice [*Azzaro*, 1999]. The high level of shallow seismicity, spatially restricted to the eastern flank of the volcano, and the analysis of the brittle deformations, indicate that this sector of Mt. Etna tends to slide towards east [*Lo Giudice and Rasà*, 1992], as confirmed by the stress field map of the area proposed by *Ferrucci et al*. [1993]. In this frame, the Pernicana and the Tremestieri faults represent the discrete structural elements embracing the seaward sliding sector [*Rasà et al.*, 1996].

The area of the Tremestieri village is extensively crossed by both an eruptive fracture and by a segment of the Tremestieri fault (Figure 1a). The eruptive fracture, named "Cavòlo Trench" [*Ferrara*, 1818] fed two historical lava flows: the "1381 eruption", whose

products outcrop in this area, and the disastrous eruption occurred in 122 BC [*Ferrara*, 1835]. The trend of this fracture is roughly NW-SE, therefore parallel to the Tremestieri fault.

The Tremestieri fault is characterized by oblique movements, with normal and dextral components of dip-slip and strike-slip displacement, respectively. This structure releases seismic energy through earthquake swarms as well as aseismic creep phenomena [*Lo Giudice and Rasà*, 1992]. Several coseismic surface faulting were observed during the April 30, 1908 earthquake [*Martinelli*, 1911] and, more recently, during the 1980 seismic sequence. Field observations during the 1980 earthquakes indicated a right-lateral and oblique displacement that implied a left stepping secondary system of *en echelon* cracks trending N45°E accompanying the NW-SE trending ruptures [*Azzaro*, 1999].

To the north, the Pernicana fault has been recognized as one of the most important and active tectonic structure of the volcano (Figure 1a). It crosses the north-eastern flank of Mt. Etna for a length of at least 11 Km, predominantly WNW-ESE trending. Its geometry, kinematics and the remarkably high slip-rate (4 cm/yr from 1980 to date), indicate that it plays a key role in controlling the instability of the volcano's eastern flank, and probably represents the northern boundary of its unstable sector [*Azzaro et al*., 2001]. The seismic activity affects essentially the climbing sector of the fault, causing damage in the Piano Pernicana area and coseismic ruptures along the fault trace. The most relevant coseismic faulting is related to the 1985 and 1986 earthquakes, when surface ruptures were observed in the western segment of the fault for a length of about 4 km, showing both extensional and vertical components of movement [*Azzaro*, 1999]. At a lower altitude, the easternmost sector of the Pernicana fault, does not show seismicity and is active only by creep motion [*Rasà et al*., 1996]. The local structural pattern, close to the village of Vena (Figure 1a),

consists of two main purely left-lateral faults, and other secondary structures that cause frequent damage to the road between the two main faults.

Seven kilometres south of Vena, the Moscarello fault develops for a length of 13 Km. It represents one of the most active faults of the Timpe system (Figure 1a), as inferred from geological and seismological evidences. It is a N20°W trending, east dipping normal fault showing no relevant strike-slip components of displacement [*Azzaro et al.*, 2000]. Significant rupture episodes have been frequently observed along the fault scarp during the 1865, 1908, 1911, 1971 earthquakes and the 1973 and 1986 seismic sequences [*Azzaro*, 1999].

A few kilometres south-west of the Timpe system, the N05°E trending Acicatena fault (Figure 1a), develops for a length of 12 km. It is characterized by a normal dip-slip with right-lateral components [*Azzaro*, 2004]. The observation, since historical time, of significant creep movements interesting the village of Acicatena and the absence of shallow seismic activity, led the geologists to believe that this fault mainly moves by stable sliding [*Rasà et al.*, 1996].

3. Earthquake data

In the framework of a cooperative activity between INGV (Section of Seismology and Tectonophysics of Rome) and the Department of Geological Science (Geology and Geophysics section) of the University of Catania, ten sites with different near-surface geological conditions were instrumented with broadband Guralp40T seismometers in and around Catania. Two of them (namely CAV0 and CAV2) were installed in the Tremestieri fault area (Figure 1a). The former was deployed 230 m from the fault, the latter on the footwall of the Tremestieri fault, less than ten meters from the fault scarp. Another station

(UNIV in Figure 1a) was installed in downtown Catania, inside the University building, on a concrete peer that since 1967 was arranged for being a node of the international gravimetric network. Its distance from CAV0 and CAV2 is about 7 km. Because of its geological structure, UNIV has been used as a reference station in our study: well logs show that 15-m thick massive lavas overlay a Quaternary clayey formation that is commonly assumed as the bedrock of the Catania area [*Monaco et al.*, 2000].

The seismometers were coupled to 24–bit Reftek 72A07 digitizers. Seismological stations were synchronized through GPS timing system, data were continuously recorded with a sampling rate of 50 sps.

Out of a dataset of about 350 recordings, the seismograms of 131 events with magnitude ranging from 2.1 to 3.9 were used in our analysis (Table 1). The choice was performed on the basis of the noise level, only events showing a signal-to-noise ratio greater than 3 units, in the frequency band 0.5-10 Hz, were selected. Earthquakes included in the analysis occurred since March 1999 till December 2001. Local earthquakes mostly belong to the seismic swarm associated to the eruptive period that began on July 2001.

3.1. Spectral ratios

For both local and regional events, a significantly different spectral content between stations is noted, CAV0 and CAV2 being much richer in high frequencies than UNIV (Figure 2). While for local earthquakes this effect might be ascribed to a larger dissipation at UNIV due to the longer source-to-station path, for regional earthquakes the propagation path can be assumed to be substantially the same and the significant difference between stations can only be interpreted in terms of a near-station effect.

To quantify this local effect, the first step was the computation of conventional spectral ratios using UNIV as reference (H/H_{ref} hereonafter) [see *Tucker and King*, 1984] and horizontal-to-vertical spectral ratios (H/V) [see *Field and Jacob*, 1995]. In order to exclude a possible source of error due to uncertainties in geometrical spreading and dissipation, no distance correction was applied in computing H/H_{ref} and only regional events were used. The entire data set including local earthquakes was used to compute H/V.

Both H/H_{ref} and H/V were calculated after rotating the NS and EW components by steps of 10° from 0° (north) to 180° (south). This approach is powerful in enhancing, if any, the occurrence of site-specific directional effects. It was first applied by *Spudich et al*. [1996] to study the directional resonance due to topography irregularities at Tarzana, California, where ground acceleration reached 1.78 g during the 1989 Northridge earthquake. Using the same procedure, *Cultrera et al*. [2003] found a directional resonance in the fault zone of Nocera Umbra, central Italy, where accelerations were anomalously large repeatedly exceeding 0.5 g for moderate-magnitude normal-faulting earthquakes. In the present study, we apply the same algorithm used by *Cultrera et al*. [2003]. The horizontal plane is divided into a set of directions spaced by 10° bins from 0° (north) to 180° (south) and the pair of horizontal components is rotated by those angles. Conditioning the component directed along the defined directions, as described before, spectral ratios become a function of frequency and direction of motion. For each of the rotated components, a time window beginning 1 s before the direct S arrival was 10%-cosine tapered for a total duration of 10 s, after the trend removal. Amplitude spectra were then computed through FFT. The same procedure was applied to the vertical components. Both the horizontal and vertical amplitude spectra were smoothed with a 0.15 Hz running frequency window. The single-event directional spectral ratios were then averaged over the

available earthquake ensamble, assuming a lognormal distribution. Figure 3 shows the final result for both H/H_{ref} and H/V. The contours of the geometric mean of H/H_{ref} at CAV2 show that the amplification centered at 4 Hz is markedly directional: the peak value increases up to 12 for rotations by 30° to 50° (Figure 3a, panel in the middle) and decreases to less than 6 in the orthogonal direction (rotations by 120° to 150°). The geometric mean of the rotated H/V spectral ratios confirms the directional resonance, even though there is a broadening of the amplified frequency band and a significant amplitude reduction from 12 to 3 in the mean value of the 4-Hz peak (Figure 3b).

The same analysis was performed for the events recorded at CAV0. When the geometric mean of H/H_{ref} spectral ratios is taken into account, the 4-Hz peak is again evident around N40°E (Figure 3a). However, the average maximum amplitude is 5 in the frequency band 3-5 Hz. Moreover, this peak at CAV0 is no more evident in the H/V spectral ratios. After analyzing the vertical component data, we can ascribe this effect to an amplification of the vertical component at CAV0 of the same order of magnitude of the horizontal components, compared to UNIV. A similar amplification of the vertical component occurs also at CAV2 but, in the frequency band 3-5 Hz, the horizontal amplification of CAV2 is significantly larger than the vertical one. Note that CAV0 (see H/H_{ref} in Figure 3) is also amplified in the frequency band 7-8 Hz, with no significant variation as a function of the rotation angle. This explains the largest amplitudes of CAV0 in Figure 2.

In the H/V spectral ratio of CAV0, the dominant peak is found at 1.8 Hz, with amplitude of about 3. This weak spectral peak is quite common in the study area and has been interpreted in terms of a resonance effect due to the local stratigraphy [*Lombardo and Rigano*, 2006]. This resonance attains a factor of about 3.5 in the H/H_{ref} panel of CAV0.

3.2. Polarization of horizontal motions during earthquakes

Rotated H/H_{ref} spectral ratios are a powerful tool to recognize directional amplifications [*Spudich et al.*, 1996; *Cultrera et al.*, 2003]. However, this approach provides a relative estimate and may then be biased by the denominator behaviour. A direct estimate of the polarization angle can be achieved by using the covariance matrix method [*Jurkevics*, 1988]. This analysis is based on the evaluation of eigenvectors and eigenvalues of the covariance matrix obtained by three component seismograms.

We have applied the code *POLARSAC* (courtesy by Mario La Rocca) to compute incidence, azimuth and rectilinearity of polarization using the eigenvector associated with the highest eigenvalue and the three eigenvalues. The polarization incidence is the angle between the polarization vector and the vertical axis, and the polarization azimuth is the angle between the projection on the horizontal plane of this vector and north, measured clockwise. The rectilinearity is calculated as

$$RL = 1 - (\lambda_2 + \lambda_3)/2\lambda_1$$

where $\lambda_1 \geq \lambda_2 \geq \lambda_3$ are the three eigenvalues of the covariance matrix [*La Rocca et al.*, 2004]. It takes values between 0 (spherical motion) and 1 (rectilinear motion).

The results of this analysis for stations CAV0, CAV2, and UNIV, after bandpass filtering in the frequency band 3-5 Hz, are shown in Figure 4. We selected two local (# 62, 126) and five regional (# 40, 103, 113, 118, 121) earthquakes with $M \geq 2.8$ (Table 1). Moving windows were 1-s long with 20% overlap. The reference station UNIV shows a complex polarization pattern that varies event by event, depending on source azimuth, fault mechanism and mode conversions along the path. In contrast, the rose-diagrams of polarization at CAV0 and CAV2 indicate a very narrow distribution. The two stations are

characterized by a persistent polarization between 40° and 50° that is independent of source azimuth and depth, suggesting a near-station origin for this effect. It is noteworthy to observe that the polarization azimuth is slightly more scattered at CAV0 rather than at CAV2 (see also Figure 5). It has also to be remarked that there is no difference in polarization between local and regional earthquakes as well as among different seismogram portions. Figure 5 also shows that at CAV2 the rectilinearity parameter is much closer to 1 than at CAV0. Also polarization incidence shows a slight difference between CAV0 and CAV2: the latter stably assumes values larger than 70° a few seconds after the direct P wave, which is the unique phase to be characterized by a vertical incidence. The lower values of polarization incidence at CAV0 are consistent with the smaller values of the H/V spectral ratios. In seismograms of CAV2, there is no way to distinguish the different phase arrivals: the entire records seem to be controlled by a strong scattering, probably caused by heterogeneities associated to near-surface damaged lava.

4. Polarization of ambient noise in the Tremestieri fault zone

H/V spectral ratios computed on ambient noise recordings are often very consistent with those derived from earthquake waveforms (see *Bard*, [1999] for a review). This is particularly true for soft sites where the fundamental resonance frequency is well peaked when the impedance contrast is sufficiently high. However, overtones disappear in the H/V spectral ratios. Theoretical explanations are proposed in the literature [*Sherbaum et al.*, 2000; *Fäh et al.*, 2001; *Bonnefoy-Claudet et al.*, 2004]. There are further structural situations prone to ground motion amplification (e.g., topography irregularities) that also show similar results in earthquake and ambient noise H/V spectral ratios [*Lermo and*

Chavez Garcia, 1993; *Caserta et al*., 2002], even though no physical model has been proposed so far to provide a theoretical background to observations.

In order to test if the results from earthquakes at stations CAV0 and CAV2 are confirmed when ambient noise is used, we measured microtremors at the same stations (namely measurement #51 and #17), a few meters from CAV0 and CAV2, respectively. Portable recording equipment is composed of a three component 1-Hz Mark L4C 3-D seismometer connected to a 12-bit analog-to-digital converter and a laptop. The observed frequency band of amplification justifies the use of 1-Hz receivers. Sampling rate was 100 sps. At each site, a 500-s long time history was recorded. From the entire time history, 25 time windows are extracted for the spectral analysis, 20-s long each one. Every time window is detrended and a 10% cosine taper is applied. The Fourier amplitude spectra are computed in the frequency band 0.5-10 Hz. Each spectrum is smoothed using a 0.25 Hz running frequency window. The H/V spectral ratios are plotted as a function of frequency and direction of motion, using the same procedure applied to earthquake-induced ground motions. The geometric average is made over the 25 selected time windows of ambient noise. All measurements were in free-field, in different hours of the day.

In Figure 6, the comparison between the rotated H/V spectral ratios from ambient noise (b) and from earthquakes (a) is shown. At site #17 (close to CAV2), the contouring of geometrical mean of H/V spectral ratios shows an amplification pattern very similar to the one obtained from earthquakes, although the 4-Hz peak is not the prevalent one and peaks at 2 and 6 Hz are more pronounced. At site #51 (close to CAV0), the rotated H/V spectral ratio from ambient noise confirms the peak at 1.8 Hz, with a similar amplitude of earthquakes. Note that the difference between #51 and #17 (using ambient noise) is less pronounced than between CAV0 and CAV2 (using earthquakes). In general, H/V spectral

ratios of ambient noise show a broader band effect with several adjacent peaks, and the variation versus azimuth is more evident than in earthquake H/V.

Based on these results and because of simplicity and low cost of ambient noise acquisition, we have extended measurements to other 18 different sites in a 1-km wide area, along and across the Tremestieri fault, intensifying measurements in zones with evidence of strong ground deformation due to the fault activity (Figure 7). In the whole area there is a predominant tendency of ground motion to be oriented at angles close to those of CAV0 and CAV2, with horizontal amplitudes 2 to 5 times larger than the vertical motion. As already observed in Figure 6, the H/V spectral ratios do not result in a narrow frequency band of amplification but tend to produce multiple adjacent peaks, spreading over the 1-10 Hz frequency band and maintaining a similar polarization. To visualize the pattern of polarization angle in the Tremestieri area we also plot the rose diagrams, after band-pass filtering data in a broad frequency band (1-10 Hz). Figure 8 confirms how narrow the distribution is in the entire study area, up to many hundreds of meters from the Tremestieri fault. The predominant direction is confirmed to be NE-SW, approximately, although several stations tend to rotate their polarization azimuth toward EW, mostly in the easternmost part of the investigated area.

4.1. Polarization of ambient noise in the Pernicana, Moscarello and Acicatena fault zones

Figure 8 gives a clear indication that ambient noise is affected by a significant horizontal polarization at the measurement sites along and across the Tremestieri fault, similarly to earthquake-induced ground motions. In order to investigate whether this property of ambient noise is recurrent on other faults, we performed microtremor surveys

on the Pernicana, Moscarello and Acicatena faults, which are characterized by different strike, direction of local stress field, and orientation of fractures [*Azzaro*, 2004].

Along the Pernicana fault, three transects (aa', bb', cc' in Figure 9) were explored, in portions of the fault where the effects of creeping and coseismic deformation are particularly evident. Again, the results indicate a systematic tendency of ambient noise to be polarized. The direction of motion varies, in this case, from NW-SE to N-S, the southernmost stations (#9 of cc' and 16 of aa') tending to rotate to an EW orientation. However, polarization persists at stations that are more than 1 kilometer far from the fault escarpment. Note that station #16 (Figure 9a) is close to the northernmost segment of the Moscarello fault.

The observed variations of polarization gave us the opportunity of testing reliability and reproducibility of results of microtremor measurements made in different hours and days. In principle, in a volcanic area, polarization could be source dependent and time dependent and we must rule out this possibility. To this purpose, we selected two sites (namely # 12 and 16, about five kilometres away each other) characterized by a different rose diagram in the not simultaneous measurements of Figure 9. We repeated microtremor measurements at the two sites simultaneously (Figure 10). Beginning at 11:30 a. m. (mostly cultural noise) up to 8:30 p. m. (natural noise), we recorded time windows of 25 minutes every hour. No significant variations in polarization were found as a function of time at station #12, and only slight variability is observed at station #16. However, the average in the entire recording period fully confirms the stability of results at both sites. A possible cause for different orientation of polarization at station #16, close to the Moscarello fault, will be discussed in the following.

The results of the check of Figure 10 suggest that polarization estimates are fairly stable and the simultaneous difference at distances of the order of several kilometers rules out the hypothesis that the observed narrow distributions are due to an incident polarized wave field generated by a volcanic source. To further confirm that our observations are not controlled by the tremor source, we performed measurements as close as possible to the tremor source area as localized by *Di Grazia et al*. [2006]. The results (see diagrams N1, N2 and N3 in Figure 9) show a polarization different from the prevailing one found along and across the Pernicana fault, although distance is less than a ten kilometers.

Two temporary seismological stations were run for a couple of months near the Pernicana fault. One was installed two kilometres east of the village of Vena (Station PER in Figure 9), and the other (PPZ) at the site of measurement # 10 of transect cc' (Figure 9c). The analysis of earthquakes recorded at these stations confirms a horizontal ground motion polarization similar to the ambient noise one (both shown in Figure 9).

Ambient noise was also recorded along two transects crossing the Moscarello fault (Figure 11) located about 15 Km to the NE of Tremestieri fault. This tectonic structure belongs to the Timpe system and develops south of the Pernicana fault: measurement #16 appears in both Figures 9a and 11. The horizontal polarization analysis shows, also for this fault, a tendency of the ambient noise to be polarized fairly uniformly. There are two prevalent directions: in the transect aa' an E-W trend prevails whereas polarization tends to rotate NE-SW to the south, in the bb' transect. The latter is also the prevalent polarization in the Tremestieri fault zone.

Finally, ambient noise measurements were performed along three transects perpendicular to the strike of the Acicatena fault (Figure 12). Polarization effects are

evident in this area as well. The prevalent trend is in E-W and NE-SW directions, although a few NW-SE polarizations are observed, especially in the southernmost part of the fault.

5. Discussion and conclusions

The results found from the earthquake and ambient noise analysis indicate that:

i) at two stations in the Tremestieri fault zone, the damaged lava amplifies ground motion during earthquakes compared to a massive lava station, amplification being independent of source azimuth and incidence angle;

ii) the effect implies a persistent, approximately NE-SW oriented polarization in the horizontal plane;

iii) ambient noise shows a polarization very similar to the one induced by earthquakes, and this ground motion peculiarity persists kilometres far from the fault;

iv) the tendency of ambient noise to be strongly polarized along the Tremestieri fault is confirmed on several transects across other three faults of Mt. Etna, the Pernicana, Moscarello and Acicatena faults, all characterized by strong tectonics. We have also found evidence of polarization of earthquake-induced ground motions, at least on the Pernicana fault;

v) in all of the faults, polarization is found to be not parallel to the fault strike.

The former [*(i)* and *(ii)*] of the above listed issues are not new: the occurrence of directional ground motion amplifications in fault zones is well documented in the literature [e.g., *Peng et al*., 2002; *Cultrera et al*., 2003]. In contrast, very few papers dealt with microtremors in fault zones, after the pioneering work by *Irikura and Kawanaka* [1980] who first inferred that vertical discontinuities can affect ambient noise characteristics. These authors observed lateral variations of the noise spectral structure when crossing a

fault in the southern part of the Kyoto basin, explaining observations in terms of reflection and transmission of surface waves through the lateral discontinuity. In our study, we find an evident persistent effect of ambient noise polarization that varies from fault to fault on Mt. Etna volcano in a strong tectonic activity area.

Although *i)* and *ii)* recall fault-guided waves, we believe that the energy trapping model (previously hypothesized by *Lombardo and Rigano* [2006]) does not fit the totality of our observations. There are many features that led to this conclusion. The two stations near the Tremestieri fault do not show seismograms where amplitude increases after direct S waves in a suite of dispersed wave trains (this is typical of fault-guided waves, see *Li et al.* [2000], among many others). Earthquake waveforms (Figure 2) rather show a continuous, persistent increment of high-frequency amplitudes along the entire seismogram. Also, polarized motions are not parallel to the fault strike as it would be expected for fault-guided waves that are composed of surface waves channelled in the wave-guide [*Rovelli et al*., 2002; *Lewis et al*., 2005].

Other critical issues for the investigated faults of Mt. Etna deal with geometry and velocity contrast of the trapping zone. Many authors assert that the trapping portion of the fault is shallow, of the order of 3 km or less (*Ben-Zion et al.* [2003], in the Karadere-Duzce branch of the North Anatolian fault; *Michael and Ben-Zion* [1998], in the Parkfield segment of the San Andreas fault; *Peng et al.* [2003], in the rupture zone of the Landers earthquake; *Lewis et al.* [2005], in the San Jacinto fault zone near Anza, California; *Rovelli et al.* [2002], in a dormant fault near Nocera Umbra, central Italy). These authors all interpret the shallow trapping portion of the fault as the top part of tectonic structures of regional extent that produce a broad (100 to 200 m) zone of damaged rock. The velocity contrast between damaged and massive rock is usually in the range 30% to 50%.

Faults of Mt. Etna depict a completely different scenario. They are the result of a recent tectonic activity and develop for a ten of kilometres (Table 2). Therefore, it is expected that the boundaries of the damaged zone are not as well defined as they can be in regional fault systems, and their width is expected to be significantly smaller. Consequently, impedance contrast and fault zone width should be very small. This is not consistent with both the resonant frequency of 4 Hz (that is typical of faults as large as 100 to 200 m) and the high amplification near the Tremestieri fault escarpment (up to a factor of 10). Moreover, the ambient noise polarization on Mt. Etna faults persists too far away from the fault trace, excluding an effect limited to a narrow low velocity zone hosted between harder wall rocks. Preliminary ambient noise measurements in other sectors of Mt. Etna (Ragalna fault and western flank of the volcano near Bronte, see Figure 13) suggest that the polarization effect is still present in fault zones of the southwestern flank whereas decreases in intensity on the western flank, where tectonic deformation is smaller. Moreover, the inspection of Figure 13 puts into evidence that the Pernicana fault seems to separates two sectors characterized by different polarization. The pattern of ground motion polarization observed to the north of the Pernicana fault (see Figures 9 and 13) is indeed more homogeneous, with prevalent NW-SE to N-S directions whereas, south of such fault, the polarization azimuth shows a high variability, even at small distances, with prevalent directions from NE-SW to E-W.

Unfortunately it is difficult to formulate an interpretative model for our observations. We do not find any evident correlation between polarization directions and strike and, when available, fracture orientation (Table 2). A possible insight could come from the results of velocity anisotropy in the Mt. Etna area [*Bianco et al*., 1996; *Bianco and Zaccarelli*, 2007]. We observe that the directions of largest velocity found in this papers

match the predominant polarization observed along the Pernicana fault (Figure 13). However, the anisotropy derived by *Bianco et al.* [1996] is relative to an about 4-km deep crustal volume beneath the southeastern flank of Mt. Etna where, at the surface, we find a different polarization azimuth. Nevertheless, anisotropy remains an appealing key of interpretation. In recent papers, *Bones and Zoback* [2006], *Cochran et al.* [2006], and *Liu et al.* [2008] study the shear-wave splitting in the San Andreas fault. They find a fast shear wave velocity direction being nearly fault-parallel for stations located on the main fault trace (structural anisotropy), and roughly parallel to the regional maximum horizontal compressive stress direction for stations outside of the damaged zone (stress-induced anisotropy). Our findings of a strong polarization in ambient noise suggests that the effect is particularly pronounced near the surface. If ambient noise is predominantly composed of randomly propagating Rayleigh waves, the smaller attenuation in the faster velocity direction could cause larger amplitudes in that direction. Considering the wave lengths at frequencies of few Hz and velocities of the order of 1 km/s, attenuation anisotropy should act in the uppermost 100 to 300 m, consistently with findings by *Liu et al.* [2005]. These authors estimate 30% of attenuation anisotropy in the uppermost 200 m of the crust, at the downhole station CHY in Taiwan. They ascribed this variation of attenuation to microfracture alignment and in situ stress, the same conditions that cause a velocity anisotropy as large as 8% at the same station [*Liu et al.*, 2005]. Anisotropy in fault zone was also investigated by *Cochran et al.* [2003], who estimated a 5% velocity anisotropy in a 2-km wide zone across two fault segments that ruptured during the Hector Mine earthquake, where the orientation of fast directions was in the middle between the fault strike and the regional stress direction. *Cochran et al.* [2003] also found that the higher the slip release on the fault, the higher the local amount of anisotropy, suggesting that a cause

for the increase of anisotropy close to the fault could be the crack opening in response to rupture during earthquakes.

Assuming that ambient noise polarization on Mt. Etna is caused by a shallow attenuation anisotropy, the same observation during earthquakes could be due to the predominance of locally scattered waves from the fault near-surface heterogeneities. Indeed the stability versus time of polarization incidence and azimuth (Figure 5) suggests that crustal phase arrivals are masked by the intense locally scattered wave field, as discussed above.

Other interpretations, although possible, are weaker. One is in terms of topography, it comes out from the observation of polarization angles roughly parallel to volcano's isolines. This is particularly true for the Pernicana and Tremestieri faults. Effects of topography on ground motion polarization are discussed in *Spudich et al*. [1996] and Gledhill [1990] However, measurements near Bronte (on the western flank) and on the Moscarello fault (Figure 13) contradict this hypothesis. Moreover, in the study area, topography is often changing at different scales but polarization angles do not change as a function of frequency in the rotated H/V spectral ratios (see Figure 7). We also made close measurements at sites with sharply varying topographical conditions and the resulting polarization did remain quite stable.

Another possible interpretation could be that polarization is normal to the fault strike. This is particularly true for the Pernicana, Moscarello and Acicatena faults. Table 2 indicates the average polarization found for each fault compared to the strike (note that the three transects on the Pernicana fault cross sectors having a different strike). Normal polarization could be consistent with an inplane resonance of seismic waves in the fault zone. However the mechanism of this resonance is not clear. This possible resonance is not

restricted to a narrow zone adjacent to the fault: stable polarization is found up to stations as distant as kilometres from the fault escarpment. *Peng and Ben-Zion* [2004] analysing the crustal anisotropy along the Karadere-Düzce branch of the North Anatolian fault, suggested the existence of a 1-km broad zone with fault-parallel cracks or shear fabric. They also observed scattered polarization directions that sometimes are almost perpendicular to the local fault strike.

On the basis of the available information, every interpretation is purely speculative. Further investigations on material properties including laboratory tests on anisotropy of fault lava samples and measurements of local attenuation in the study area are already in progress.

Acknowledgements

The authors wish to thank an anonymous reviewer and the Associate Editor for constructive comments which contributed to improve the quality of the paper. Special thanks to Francesca Bianco for useful discussions and critical reading of the manuscript. This work was carried out with internal research funds of Department of Geological Sciences of the Catania University and Istituto Nazionale di Geofisica e Vulcanologia, Department of Seismology and Tectonophysics of Rome. A partial contribution came from Project S3 "Scenari di scuotimento e di danno atteso in aree di interesse prioritario e/o strategico" of the 2005-2007 DPC-INGV research programs.

References

Azzaro, R. (1999), Earthquake surface faulting at Mount Etna volcano (Sicily) and implications for active tectonics, *J. Geodyn*., 28, 193-213.

Azzaro, R., L. Ferreli, A. M. Michetti, L. Serva, E. Vittori (1998), Environmental hazard of capable faults: the case of the Pernicana fault (Mt. Etna, Sicily), *Natural Hazard*, 17, 147-162.

Azzaro, R., D. Bella, L. Ferreli, A. M. Michetti, F. Santagati, L. Serva, E. Vittori (2000), First study of fault trench stratigraphy at Mt. Etna volcano, Southern Italy: understanding Holocene surface faulting along the Moscarello fault, *J. Geodyn*., 29 (3-5), 187-210.

Azzaro, R., M. Mattia, G. Puglisi (2001), Dynamics of fault creep and kinematics of the eastern segment of the Pernicana fault (Mt. Etna, Sicily) derived from geodetic observations and their tectonic significance, *Tectonophysics*, 333 (3-4), 401-415.

Azzaro, R. (2004), Seismicity and active tectonics in the Etna region: constraints for a seismotectonic model, in *Mt. Etna: volcano laboratory,* vol. 143, edited by A. Bonaccorso, S. Calvari, M. Coltelli, C. Del Negro and S. Falsaperla, pp. 205-219, AGU monograph.

Bard, P.Y. (1999), Microtremor measurements: a tool for site effect estimation?, in *The Effects of Surface Geology on Seismic Motion*, Irikura, edited by Kudo, Okada, Sasatani, pp. 1251-1279, Balkema, Rotterdam.

Ben-Zion, Y., and K. Aki (1990), Seismic radiation from an SH line source in a laterally heterogeneous planar fault zone, *Bull. Seism. Soc. Am*., 80, 971-994.

Ben-Zion, Y., Z. Peng, D. Okaya, L. Seeber, J.G. Armbruster, N. Ozer, A.J. Michael, S. Baris, and M. Aktar (2003), A shallow fault-zone structure illuminated by trapped

waves in the Karadere-Duzce branch of the North Anatolian Fault, western Turkey, *Geophys. J. Int.*, 152, 1-19.

Bianco, F., M. Castellano, G. Milano, and G. Vilardo (1996), Shear-wave polarization alignment on the eastern flank of Mt.Etna volcano (Sicily, Italy), *Annali di Geofisica*, XXXIX, 2, 429-443.

Bianco, F., and L. Zaccarelli, A reappraisal of shear wave splitting parameters from Italian active volcanic areas through a semi-automatic algorithm. *Journal of Seismology,* in press.

Bones, N.L. and M.D. Zoback (2006), Mapping stress and structurally controlled crustal shear velocity anisotropy in California, *Geology*, 34, 10, 825-828.

Bonnefoy-Claudet, S. (2004), Nature du bruit de fond sismique: implications pour les études des effets de site, Docteur Thèse, 234 pp., Université J. Fourier – Grenoble 1, in SESAME project http://sesame-fp5.obs.ujf-grenoble.fr/.

Boore, D. M., V. M. Graizer, J. C. Tinsley, and A. F. Shaka (2004), A study of possible ground-motion amplification at the Coyote Lake dam, California, *Bull. Seism. Soc. Am.*, 94, 4, 1327-1342, doi: 10.1785/012003144l.

Caserta, A., V. Ruggiero, P. Lanucara (2002), Numerical modelling of dynamical interaction between seismic radiation and near-surface geological structures: a parallel approach, *Computers & Geosciences*, 28, 1069–1077.

Cochran, E.S., Y.-G. Li, and J. E. Vidale (2006), Anisotropy in the shallow crust observed around the San Andreas fault befor and after the 2004 M 6.0 Parkfield earthquake, *Bull. Seismol. Soc. Am.*, 96, 4B, S364-S375.

Cochran, E.S., J. E. Vidale, Y.-G. Li (2003), Near-fault anisotropy following the Hector Mine earthquake, *J. Geoph. Res.*, 108, 2436, doi: 10.1029/2002JB002352.

Cultrera, G., A. Rovelli, G. Mele, R. Azzara, A. Caserta, F. Marra (2003), Azimuth-dependent amplification of weak and strong ground motions within a fault zone (Nocera Umbra, central Italy), *J. Geoph. Res.*, 108 (B3), 2156, doi: 10.1029/2002JB001929.

Di Grazia, G., S. Falsaperla, H. Langer (2006), Volcanic tremor location during the 2004 Mount Etna lava effusion, *Geophys. Res. Lett.*, 33, L04304, doi: 10.1029/2005GL025177.

Fäh, D., F. Kind, D. Giardini (2001), A theoretical investigation on H/V ratios, *Geophys. J. Int.*, 145, 535-549.

Ferrucci, F., R. Rasà, G. Gaudiosi, R. Azzaro, and S. Imposa (1993), Mt. Etna: a model for the 1989 eruption, *J. Volcanol. Geotherm. Res*., 56, 35-56.

Ferrara, F. (1818), Descrizione dell'Etna, con la Storia delle Eruzioni e il Catalogo dei Prodotti, pp. 256, Lorenzo Dato, Palermo.

Ferrara, F. (1835), Sopra la eruzione dell'Etna segnata da Orosio nel 122 innanzi G.C., *Atti Accad. Gioenia Sci. Nat*., Catania I 10, 141-158.

Field, E. H., and K. H. Jacob (1995), A comparison and test of various site response estimation techniques, including three that are not reference site dependent, *Bull. Seism. Soc. Am*., 85, 1127-1143.

Gledhill, K.R. (1990), A shear-wave polarization study in the Wellington region New Zealand, *Geophys. Res. Lett.*, 17, 9, 1319-1322

Igel, H., G. Jahnke, and Y. Ben-Zion (2002), Numerical simulation of fault zone trapped waves: Accuracy and 3-D effects, *Pure Appl. Geophys.*, 159, 2067-2083.

Irikura, K., T. Kawanaka (1980), Characteristics of microtremors on ground with discontinuous underground structure, *Bull. Disas. Prev. Inst. Kyoto Univ*., 30-3, 81-96.

Jahnke, J., H. Igel, and Y. Ben-Zion (2002), 3D calculations of fault zone guided waves in various irregular structures, *Geophys. J. Int*., 151, 416-426.

Jurkevics, A. (1988), Polarization analysis of three component array data, *Bull. Seism. Soc. Am*., 78, 1725-1743.

La Rocca, M., D. Galluzzo, G. Saccorotti, S. Tinti, G. B. Cimini, E. Del Pezzo (2004), Seismic signals associated with landslides and with a tsunami at Stromboli volcano, Italy, *Bull. Seism. Soc. Am*., 94 (5), 1850-1867.

Lermo, J., F. Chavez-Garcia (1993), Site effect evaluation using spectral ratios with only one station, *Bull. Seism. Soc. Am*., 83, 1574-1594.

Lewis, M. A., Z. Peng, Y. Ben-Zion, F. L. Vernon (2005),. Shallow seismic trapping structure in the San Jacinto fault zone near Anza, California, *Geophys. J. Int*., 162, 867-881.

Li, Y. G., P. C. Leary, K. Aki, and P. Malin (1990), Seismic trapped modes in the Oroville and San Andreas fault zones, *Science*, 249, 763-765.

Li, Y. G., K. Aki, D. Adams, and A. Hasemi (1994), Seismic guided waves in the fault zone of the Landers, California, earthquake of 1992, *J. Geophys. Res*., 99, 11705-11722.

Li, Y. G., and J. E. Vidale (1996), Low-velocity fault-zone guided waves: Numerical investigations of trapping efficiency, *Bull. Seism. Soc. Am*., 86, 371-378.

Li, Y. G., J. E. Vidale, K. Aki, and F. Xu (2000), Depth-dependent structure of the Landers fault zone using fault zone trapped waves generated by aftershocks, *J. Geophys. Res.*, 105**,** 6237–6254.

Liu, Y., T.-L Teng, Y. Ben-Zion (2005), Near-surface seismic anisotropy, attenuation and dispersion in the aftershock region of the 1999 Chi-Chi earthquake, *Geophys. J. Int*., 160, 695-706.

Liu, Y., H. Zhang, C. Thurber, and S. Roecker (2008), Shear wave anisotropy in the crust around the San Andreas fault near Parkfield: spatial and temporal analysis, *Geophys.J. Int*. 172, 3, 957-970.

Lo Giudice, E., and R. Rasà (1992), Very shallow earthquakes and brittle deformation in active volcanic areas: the Etnean region as example, *Tectonophysics*, 202, 257-268.

Lombardo, G., and R. Rigano (2006), Amplification of ground motion in fault and fracture zones: observations from the Tremestieri fault, Mt. Etna (Italy), *J. Volcanol. Geotherm. Res.*,153, 167-176.

Martinelli, G. (1911), Notizie sui terremoti osservati in Italia durante l'anno 1908, *App. Boll. Soc. Sism. It*., 15.

McGuire, W. J., and A. D. Pullen (1989), Location and orientation of eruptive fissures and feeder dykes at Mount Etna; influence of gravitational and regional tectonic stress regimes, *J. Volcanol. Geotherm. Res*., 38, 325-344.

Michael, A. J., Y. Ben-Zion (1998), Inverting fault zone trapped waves with genetic algorithm, *EOS, Trans. Am. Geophys. Un*., 79, F584.

Monaco, C., P. Tapponnier, L. Tortorici, P. Y. Gillot (1997), Late Quaternary slip rates on the Acireale-Piedimonte normal faults and tectonic origin of Mt. Etna (Sicily), *Earth Planet. Sci. Lett.,* 147, 125-139.

Monaco, C., S. Catalano, G. De Guidi, S. Gresta, H. Langer, and L. Tortorici (2000), The geological map of the urban area of Catania, Eastern Sicily: morphotectonic and seismotectonic implications, *Mem. Soc. Geol. It.*, 55, 425-438.

Peng, Z., and Y. Ben-Zion (2004), Systematic analysis of crustal anisotropy along the Karadere-Düzce branch of the North Anatolian fault, *Geophys. J. Int.*, 159, 253-274, doi: 10.1111/j.1365-246X.2004.02379.x.

Peng, Z., Y. Ben-Zion, A. J. Michael, and L. Zhu (2002), Quantitative analysis of seismic trapped waves in the rupture zone of the Landers, 1992, California earthquake: evidence for a shallow trapping structure, *EOS, Trans. Am. geophys. Un.*, 83.

Peng, Z., Y. Ben-Zion, L. Zhu, and A. J. Michael (2003), Inference of a shallow fault zone layer in the rupture zone of the 1992 Landers, California earthquake fro locations of events generating trapped waves and traveltime analysis. *Geophys. J. Int.*, 155**,** 1021–1041.

Rasà, R., R. Azzaro, O. Leonardi (1996), Aseismic creep on faults and flank instability at Mt. Etna volcano, Sicily, in: *Volcano Instability on the Earth and Other Planets*, Geological Society Special Publication, 110, edited by W. C. McGuire, A. P. Jones, and J. Neuberg, pp. 179-192.

Rovelli, A., A. Caserta, F. Marra, and V. Ruggiero (2002), Can seismic waves be trapped inside an inactive fault zone? The case study of Nocera Umbra, central Italy, *Bull. Seismol. Soc. Am.*, 92, 2217-2232.

Sherbaum F., K. -G. Hinzen, R. Pelzing, M. Ohrnberger, S. K. Reamer, A. Sachse, R. Streich (2000), Analysis of ambient vibrations in the Lower Rhine Embayment to study local site effects, *Eos Trans. AGU, Fall Meet. Suppl. 2000*.

Spudich, P., M. Hellweg, H. K. Lee (1996), Directional topographic site response at Tarzana observed in aftershocks of the 1994 Northridge, California, earthquake: implications for mainshock motions, *Bull. Seism. Soc. Am.*, 86, S193-S208.

Tucker, D. E., and J. L. King (1984), Dependence of sediment filled valley response on input amplitude and valley properties, *Bull. Seism. Soc. Am.*, 74, 153-165.

FIGURE CAPTIONS

Figure 1. Simplified structural setting of the study area and epicentres (open circles) of Etnean (a) and regional (b) earthquakes used in this study. The size of the open circles is proportional to the magnitude. Gray triangles indicate the location of seismic stations. In (b), the epicentres marked with numbers are relative to the earthquakes used for the polarization analysis. Major fault systems are also shown.

Figure 2. Illustrative set of three-component seismograms and spectra of local and regional earthquakes recorded at the three stations.

Figure 3. Contours of the geometric mean of spectral ratios as a function of frequency (x-axis) and direction of motion (y-axis) for earthquake recordings of stations CAV2 and CAV0. The panels in the middle represent the geometric mean, and

top and bottom panels the ±1 standard deviation patterns, respectively. (a) Earthquake conventional spectral ratios (reference site); (b) Earthquake H/V spectral ratios.

Figure 4. Rose diagrams of azimuth of horizontal polarization for earthquakes recorded at stations CAV0, CAV2 and UNIV. Statistics are made over the entire seismograms according to examples shown in Figure 5.

Figure 5. Instantaneous values of polarization azimuth, rectilinearity and polarization incidence during earthquakes at stations CAV0 and CAV2.

Figure 6. Contours of the geometric mean of H/V spectral ratios as a function of frequency (x-axis) and direction of motion (y-axis) for (a) earthquake recordings at stations CAV2 and CAV0, and (b) ambient noise (measurements # 17 and # 51). The panels in the middle represent the geometric mean, and top and bottom panels the ±1 standard deviation patterns, respectively.

Figure 7. Average ambient noise H/V spectral ratios in the Tremestieri fault area.

Figure 8. Rose diagrams of azimuth of horizontal polarization in the Tremestieri fault area. Numbers in the lower left corner of each diagram indicate the percentage of running rectilinearity values greater than 0.5.

Figure 9. Rose diagrams of azimuth of horizontal polarization in the Pernicana fault area along the three transects aa', bb' and cc' (shown in panels a, b, and c, respectively). Results of polarization analysis of ambient noise (N) and earthquake recordings (E) at stations PER and PPZ, and the rose diagrams of measurements in the summit area (N1, N2, N3) are depicted as well. Numbers in the lower left corner of each diagram indicate the percentage of running rectilinearity values greater than 0.5.

Figure 10. Rose diagrams of azimuth of horizontal polarization from hourly measurements of noise at sites 12 (a) and 16 (b), located along the transect aa' in Figure 9a. Measurements were performed simultaneously at the two sites (the hour is written in each inset).

Figure 11. Rose diagrams of azimuth of horizontal polarization in the Moscarello fault area. Numbers in the lower left corner of each diagram indicate the percentage of running rectilinearity values greater than 0.5.

Figure 12. Rose diagrams of azimuth of horizontal polarization in the Acicatena fault area. Numbers in the lower left corner of each diagram indicate the percentage of running rectilinearity values greater than 0.5.

Figure 13. Selected rose diagrams (gray squares) of ambient noise polarization in the studied faults, crater area (N2) and western flank of the volcano (A, B). The polarization of earthquakes (white squares) is also drawn. Diagrams in white circles show the results of velocity anisotropy found by *Bianco et al.* [1996] and *Bianco and Zaccarelli* [2007] using earthquakes recorded at the stations in the map (gray triangles).

Table 1. List of earthquakes used in this study. One asterisk indicates the available recordings, double asterisk means poor signal to noise ratio (not included in the spectral ratio computation).

Table 2. Geological parameters of studied faults (modified from *Azzaro* [2004]) and mean polarization angle (* the average is made over measures at stations closer than 250 m from the fault trace).

#	dd/mm/yy h	Lat. N	Long. E	Depth (Km)	M_D	CAV0	CAV2	UNIV
1	5/23/1999 11:53	37.904	14.989	4	3.3	*		*
2	6/2/1999 10:36	38.672	14.03	10	3.0	*		**
3	6/13/1999 17:45	37.786	15.961	44	3.2	*		**
4	6/22/1999 4:11	37.675	14.945	10	2.5	*		*
5	7/2/1999 22:40	37.681	14.949	10	2.4	*		
6	10/3/1999 9:33	38.255	14.746	151	3.4	*		
7	10/12/1999 1:18	37.689	14.978	2	2.3	*		**
8	10/12/1999 1:21	37.722	14.971	5	3.0	*		*
9	10/12/1999 1:29	37.719	15.018	5	2.4	*		**
10	10/12/1999 1:55	37.729	14.972	5	2.7	*		*
11	10/12/1999 3:27	37.717	14.961	5	2.7	*		*
12	10/12/1999 4:58	37.728	14.973	5	2.8	*		**
13	10/15/1999 3:13	37.126	15.089	5	2.9	*		**
14	11/20/2000 20:12	37.816	14.99	8	3.0	*		*
15	11/20/2000 23:41	37.811	14.965	9	3.3	*		*
16	1/4/2001 22:20	38.727	14.949	356	3.5	*		*
17	1/23/2001 16:54	37.133	15.33	15	3.3	*		*
18	1/26/2001 8:19	37.752	14.979	10	2.8	*		*
19	1/26/2001 8:19	37.732	14.986	5	3.2	*		*
20	1/26/2001 10:43	37.772	14.976	5	2.7	*		*
21	2/10/2001 17:45	37.158	14.993	12	2.1	*		*
22	3/7/2001 17:19	37.893	14.869	27	2.9	*		
23	3/30/2001 18:40	37.732	15.003	5	2.9	*	*	*
24	4/23/2001 17:13	37.702	15.003	5	2.5	*	*	**
25	4/23/2001 22:25	37.728	14.986	5	2.4	*	*	**
26	4/24/2001 4:03	37.716	14.983	5	2.9	*	*	*
27	4/25/2001 19:32	37.739	15.044	2	3.1	*	*	*
28	4/27/2001 21:08	37.73	15.028	5	2.4	*	*	*
29	4/28/2001 12:40	37.727	15.03	5	2.7	*	*	**
30	4/29/2001 19:59	37.773	14.962	11	3.1	*	*	*
31	5/2/2001 7:47	37.712	15.008	3	2.9	*	**	**
32	5/3/2001 21:40	37.648	14.966	5	3.2	*	*	**
33	5/3/2001 21:45	37.647	14.965	10	2.9	*	*	**
34	5/4/2001 4:41	37.628	14.959	10	3.0	*	*	**
35	5/7/2001 20:06	37.789	14.975	8	2.4	*	*	*
36	5/8/2001 3:52	38.14	14.913	9	3.3	*	*	*
37	5/9/2001 0:21	37.635	15.095	5	2.7	*	*	*
38	5/10/2001 18:25	37.716	14.933	10	2.7	*	*	**
39	5/10/2001 18:26	37.698	14.927	5	2.5	*	*	**
40	5/17/2001 11:43	38.809	15.861	284	3.6	*	*	*
41	5/19/2001 15:51	37.752	14.87	10	2.5	*	*	**
42	5/19/2001 16:14	37.764	14.876	14	3.0	*	*	*
43	5/19/2001 20:46	37.777	14.955	9	2.7	*	*	**
44	5/20/2001 20:07	37.742	14.921	5	2.9	*	*	**
45	5/26/2001 6:01	37.447	16.048	12	3.6	*	*	*
46	6/9/2001 17:49	37.747	15.133	5	2.8	*	*	**
47	6/19/2001 1:30	37.753	15.046	5	2.5	*	*	*
48	6/21/2001 1:25	37.746	14.72	9	2.6	*	*	*
49	7/8/2001 6:28	38.515	16.789	48	3.3	*	*	*
50	7/12/2001 22:39	37.51	15.002	5	2.4	*	*	**
51	7/12/2001 22:45	37.618	15.172	5	2.7	*	*	**
52	7/13/2001 0:10	37.769	15.054	5	2.8	*	*	**
53	7/13/2001 0:19	37.722	15.011	1	2.5	*	*	**
54	7/13/2001 0:39	37.674	15.047	5	2.5	*	*	**
55	7/13/2001 0:41	37.713	15.041	0	2.6	*	*	**

56	7/13/2001 1:30	37.706	15.044	1	2.8	*	*	*
57	7/13/2001 1:35	37.711	15.042	1	2.9	*	*	*
58	7/13/2001 1:38	37,652	15,029	5	2.4	*	*	**
59	7/13/2001 2:36	37.715	15.013	1	2.6	*	*	**
60	7/13/2001 2:50	37.51	15.166	5	2.5	*	*	**
61	7/13/2001 2:58	37.769	15.017	5	2.3	*	*	**
62	7/13/2001 3:12	37.654	15.107	5	3.9	*	*	*
63	7/13/2001 3:14	37.693	14.968	0	3.9	*	*	*
64	7/13/2001 3:23	37.713	15.016	1	3.0	*	*	**
65	7/13/2001 3:25	37.881	15.082	5	2.4	*	*	**
66	7/13/2001 3:34	37.724	15.01	0	2.7	*	*	**
67	7/13/2001 4:33	37.722	15.003	0	2.9	*	*	**
68	7/13/2001 4:45	37.731	14.999	1	3.1	*	*	**
69	7/13/2001 4:48	37.707	15.042	1	2.6	*	*	*
70	7/13/2001 11:54	37.716	15.016	3	3.0	*	*	*
71	7/13/2001 21:15	37.694	15.031	5	2.6	*	*	**
72	7/13/2001 21:58	37.625	15.14	5	2.5	*	*	**
73	7/14/2001 1:19	37.727	15.01	1	3.0	*	*	*
74	7/14/2001 3:04	37.694	15.046	0	3.4	*	*	**
75	7/14/2001 4:18	37.699	14.956	0	2.8	*	*	**
76	7/14/2001 4:40	37.716	14.961	4	2.9	*	*	**
77	7/14/2001 4:46	37.72	14.951	0	3.1	*	*	**
78	7/14/2001 7:37	37.692	15.051	1	3.4	*	*	**
79	7/14/2001 8:53	37.709	15.042	1	3.5	*	*	**
80	7/14/2001 12:02	37.679	14.971	4	2.5	*	*	**
81	7/14/2001 13:35	37.695	14.973	3	3.1	*	*	*
82	7/14/2001 15:18	37.671	15.009	5	2.3	*	*	**
83	7/14/2001 19:07	37.625	14.959	3	2.4	*	*	**
84	7/14/2001 21:54	37.697	14.999	0	2.8	*	*	**
85	7/15/2001 0:08	37.835	15.009	5	2.7	*	*	**
86	7/15/2001 0:10	37.701	14.97	0	3.1	*	*	*
87	7/15/2001 0:13	37.693	14.971	0	3.4	*	*	*
88	7/15/2001 1:18	37.69	14.976	0	2.9	*	*	**
89	7/15/2001 3:11	37.699	14.963	1	3.4	*	*	*
90	7/15/2001 3:27	37.649	14.971	0	3.3	*	*	**
91	7/15/2001 4:56	37.703	15.045	1	3.5	*	*	**
92	7/15/2001 5:47	37.632	14.978	0	2.8	*	*	**
93	7/15/2001 5:49	37.632	14.978	0	2.8	*	*	**
94	7/15/2001 7:44	37.732	15.002	0	3.5	*	*	**
95	7/15/2001 9:00	37.709	14.885	4	3.4	*	*	**
96	7/15/2001 10:16	37.713	14.939	5	2.5	*	**	**
97	7/15/2001 10:24	37.723	14.961	5	2.2	*	*	**
98	7/15/2001 14:40	37.715	14.949	0	3.1	*	*	**
99	7/15/2001 15:01	37.681	14.98	0	3.3	*	*	**
100	7/15/2001 23:32	37.701	15.083	4	2.6	*	*	**
101	7/15/2001 23:37	37.683	15.115	5	2.5	*	*	*
102	7/15/2001 23:40	37.707	14.936	5	2.3	*	*	**
103	7/16/2001 0:36	37.826	14.979	5	2.8	*	*	*
104	7/16/2001 2:43	37.714	15.014	0	3.1	*	*	**
105	7/16/2001 3:59	37.717	15.005	0	3.1	*	*	**
106	7/16/2001 12:48	37.67	15.017	10	2.5	*	*	
107	7/18/2001 19:59	37.705	14.917	5	2.7	*	*	
108	7/19/2001 12:16	37.656	15.115	5	2.4	*	*	
109	7/21/2001 23:41	37.69	15.096	3	2.6	*	*	**
110	7/22/2001 12:31	37.689	15.06	0	3.3	*	*	**
111	7/23/2001 20:41	37.64	15.125	0	2.6	*	*	**

112	7/31/2001 18:46	38.488	15.16	6	3.5	*	*	*
113	8/17/2001 3:14	38.343	14.729	231		*	*	*
114	8/20/2001 22:44	37.711	15.078	3	3.3	*	*	*
115	8/21/2001 1:54	37.71	15.081	5	2.6	*	*	**
116	8/30/2001 16:17	37.598	15.112	10	2.3		*	
117	8/30/2001 22:08	37.474	15.154	10	2.3		*	**
118	9/14/2001 18:53	37.524	16.113	17	3.4		*	*
119	9/30/2001 16:55	37.649	13.974	15	3.0		*	*
120	10/15/2001 20:43	37.584	15.169	5	2.6		*	**
121	10/18/2001 11:01	39.259	16.278	5			*	*
122	10/18/2001 18:07	38.494	15.132	246			*	*
123	10/19/2001 22:35	37.616	14.141	20	2.8		*	*
124	10/26/2001 5:37	37.636	15.162	4	2.9		*	**
125	10/28/2001 9:03	37.594	15.17	5	3.7		*	**
126	10/28/2001 15:04	37.614	15.139	5			*	**
127	10/31/2001 22:05	37.605	15.181	5	2.5		*	**
128	10/31/2001 23:43	37.618	15.141	5	2.5		*	**
129	11/3/2001 14:52	37.752	14.732	6	2.7		*	*
130	11/5/2001 4:17	37.719	14.613	19	2.3		*	
131	12/12/2001 11:05	37.595	15.157	10	2.5		*	**

Faults	Length (km)	Strike	Faulting style	N. measures*	Polarization angle
Acicatena	12	5°	Normal, with right-lateral comp.	14	86°±10°
Moscarello	13	160°	Normal, with minor dextral slip	12	71°±8°
Pernicana	11				
aa'		105°	Oblique, sinistral strike slip	9	108°±23°
bb'		95°		6	119°±23°
cc'		90°		8	134°±8°
Ragalna	6.5	60°	Normal	4	96°±17°
Tremestieri	7.3	135°	Dextral, oblique strike slip	17	67°±4°

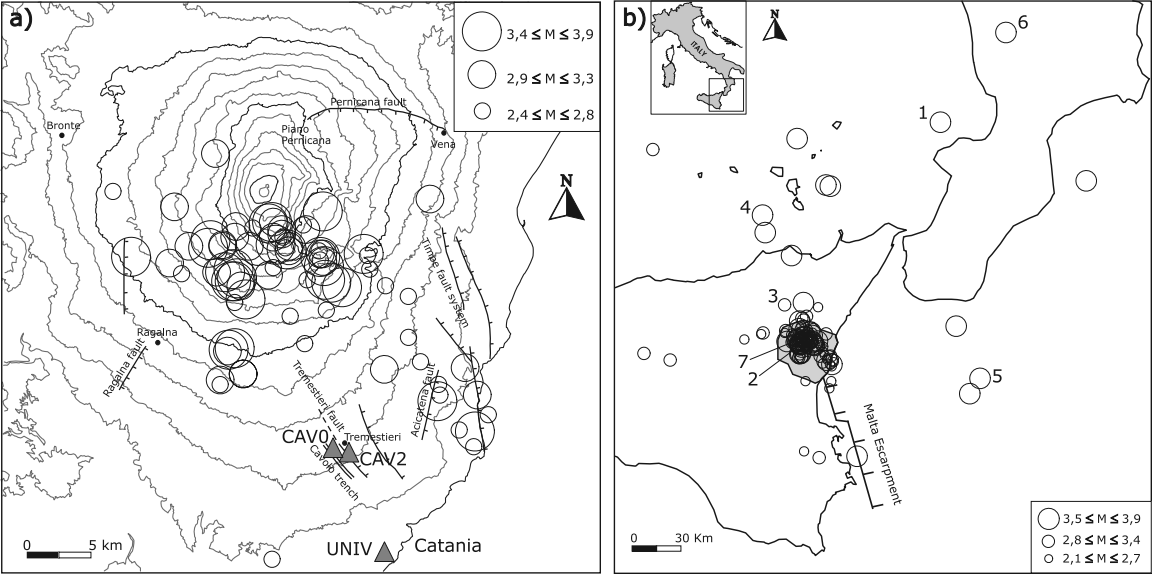
a)
3,4 ≤ M ≤ 3,9
2,9 ≤ M ≤ 3,3
2,4 ≤ M ≤ 2,8
Pernicana fault
Piano Pernicana
Bronte
Vena
N
Timpe fault system
Ragalna
Ragalna fault
Tremestieri fault
Tremestieri
Acicastello fault
CAV0
CAV2
Cavo trench
0
5 km
UNIV
Catania
b)
ITALY
N
6
1
4
3
7
2
5
Malta Escarpment
0
30 Km
3,5 ≤ M ≤ 3,9
2,8 ≤ M ≤ 3,4
2,1 ≤ M ≤ 2,7

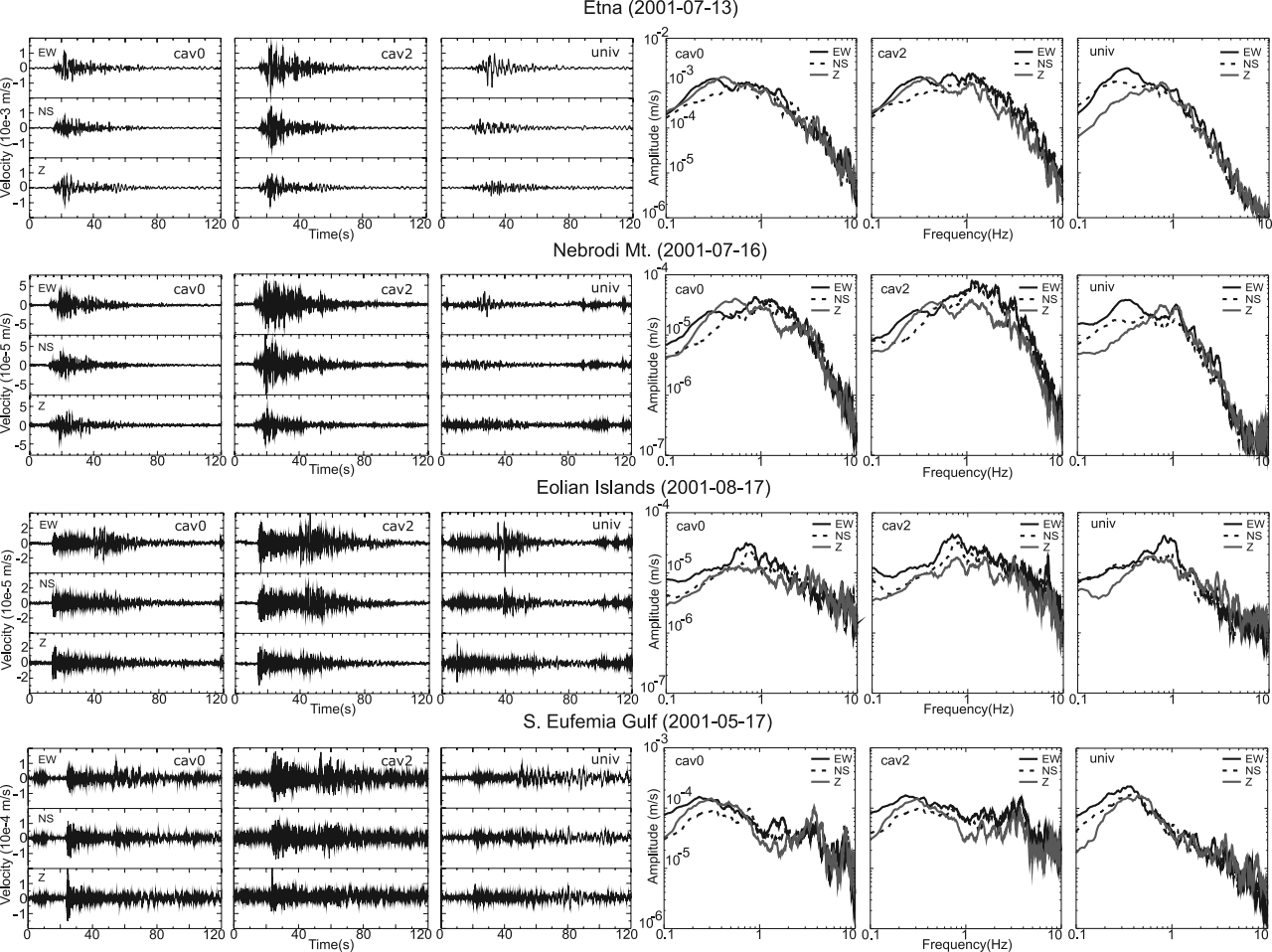
Etna (2001-07-13)
Nebrodi Mt. (2001-07-16)
Eolian Islands (2001-08-17)
S. Eufemia Gulf (2001-05-17)
cav0
cav2
univ
EW
NS
Z
Velocity (10e-3 m/s)
Velocity (10e-5 m/s)
Velocity (10e-4 m/s)
Amplitude (m/s)
Time(s)
Frequency(Hz)

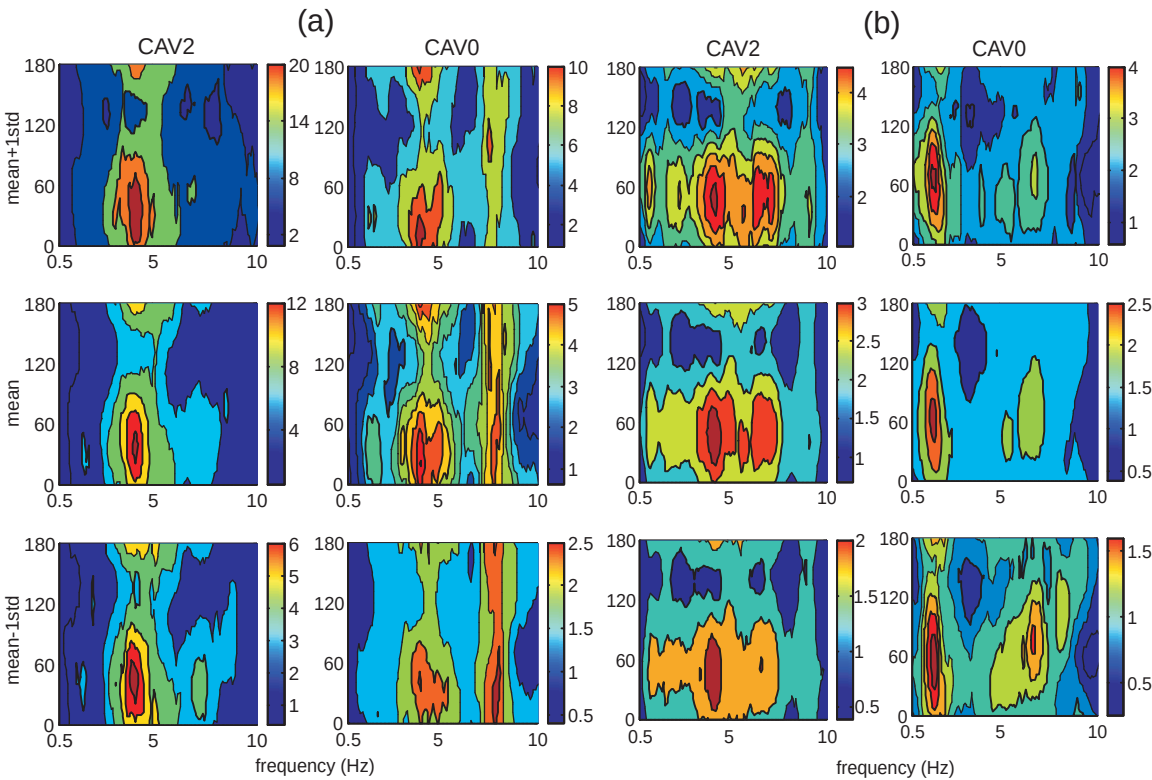
(a)
(b)
CAV2
CAV0
CAV2
CAV0
mean+1std
mean
mean-1std
frequency (Hz)
frequency (Hz)

S. Eufemia Gulf (2001-05-17)

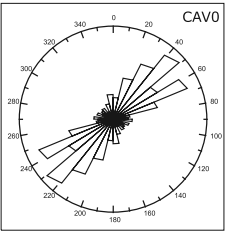

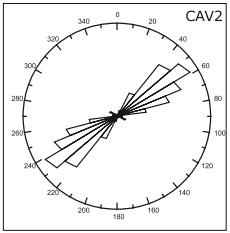

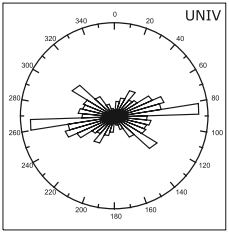

Ionian Sea (2001-09-14)

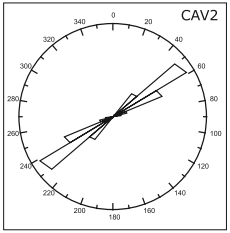

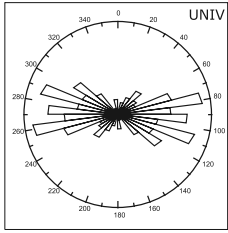

Etna (2001-07-13)

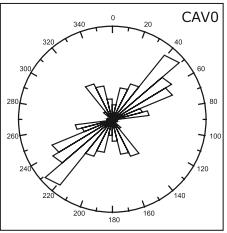

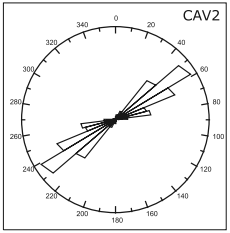

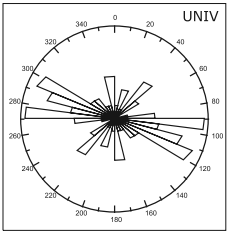

Sila (2001-10-18)

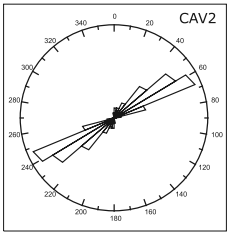

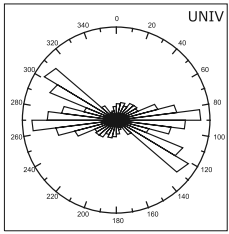

Nebrodi Mt. (2001-07-16)

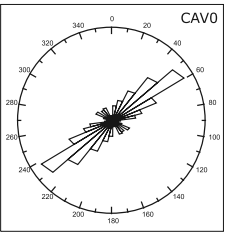

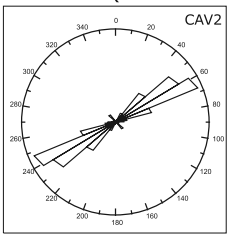

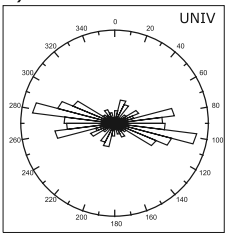

Etna (2001-10-28)

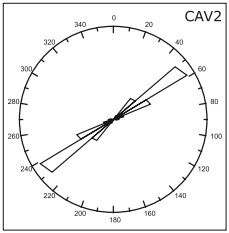

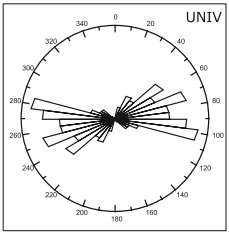

Eolian Islands (2001-08-17)

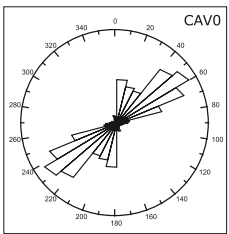

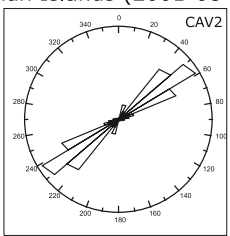

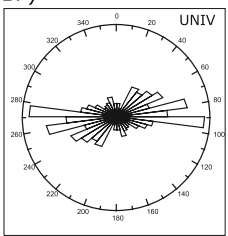

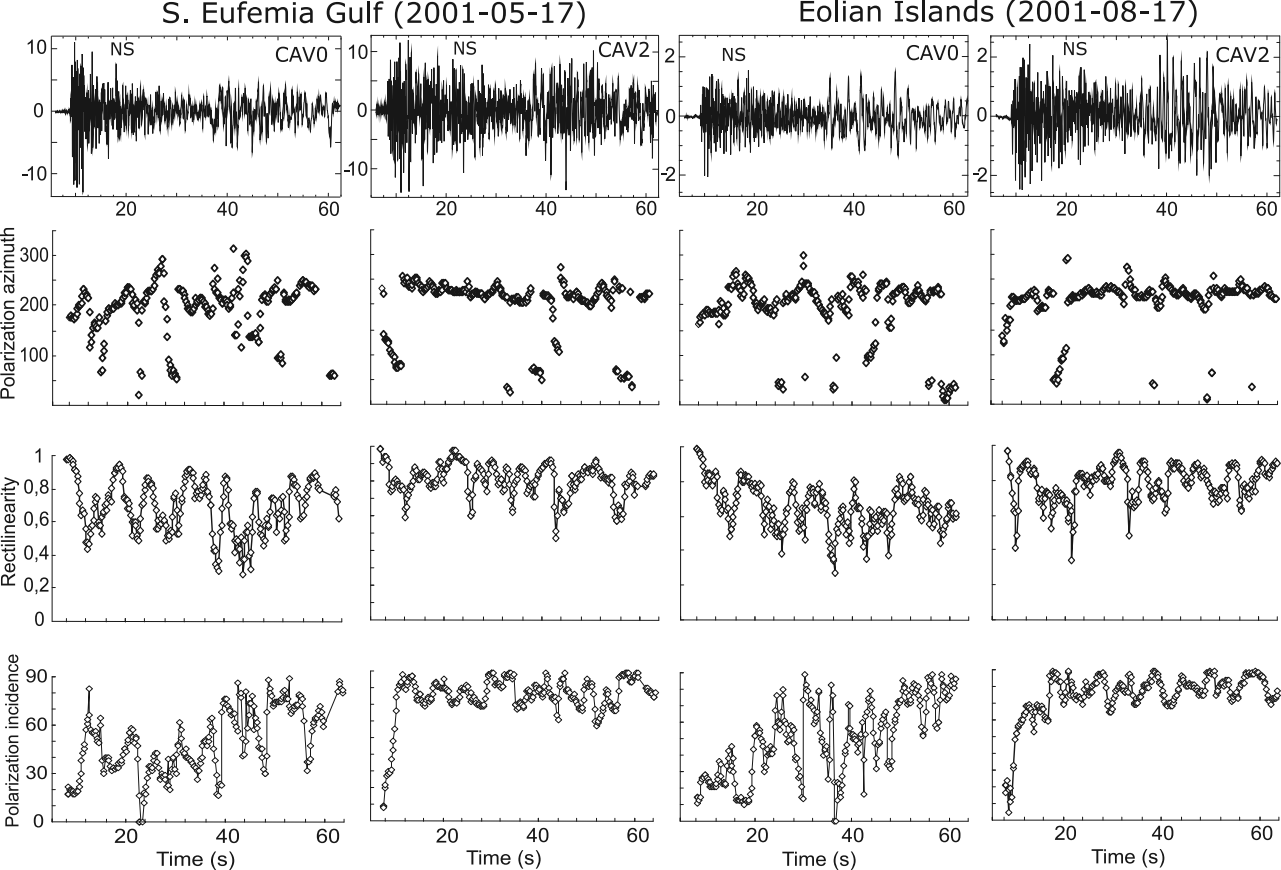
S. Eufemia Gulf (2001-05-17)
Eolian Islands (2001-08-17)
NS
CAV0
CAV2
Polarization azimuth
Rectilinearity
Polarization incidence
Time (s)

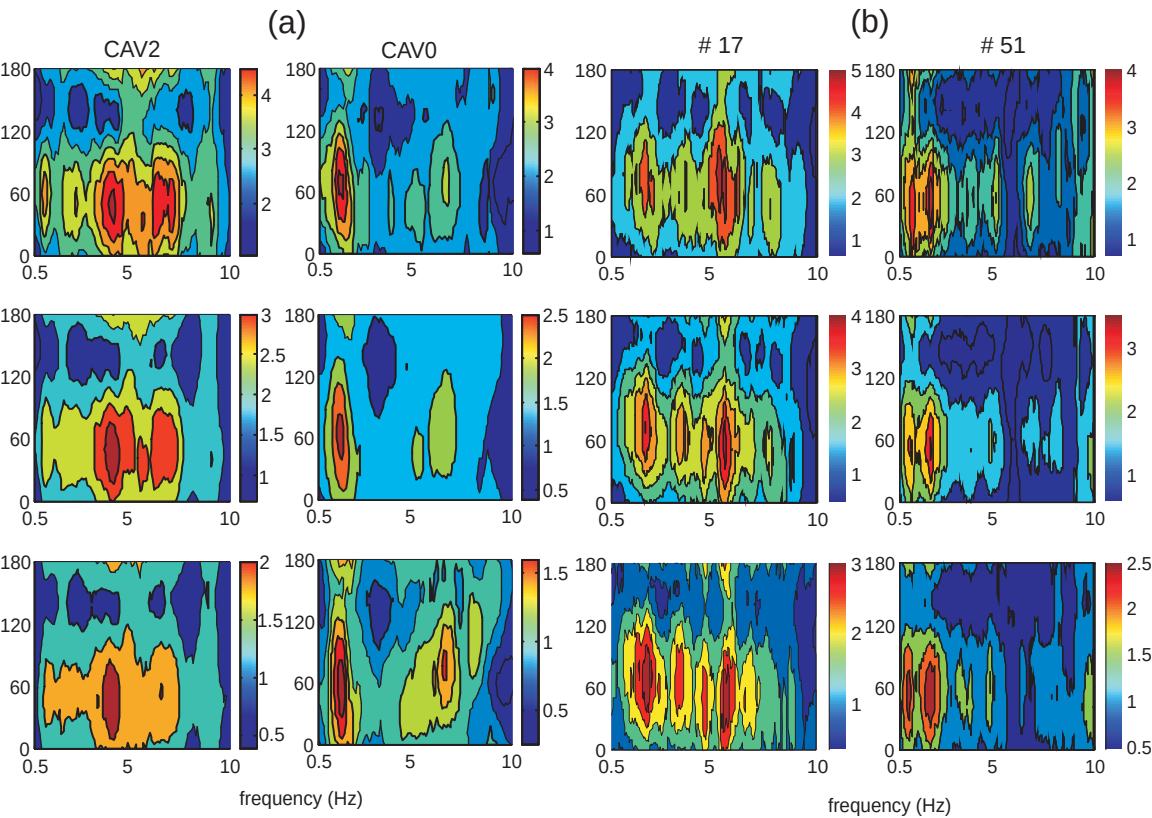
(a)
(b)
CAV2
CAV0
17
51
frequency (Hz)
frequency (Hz)

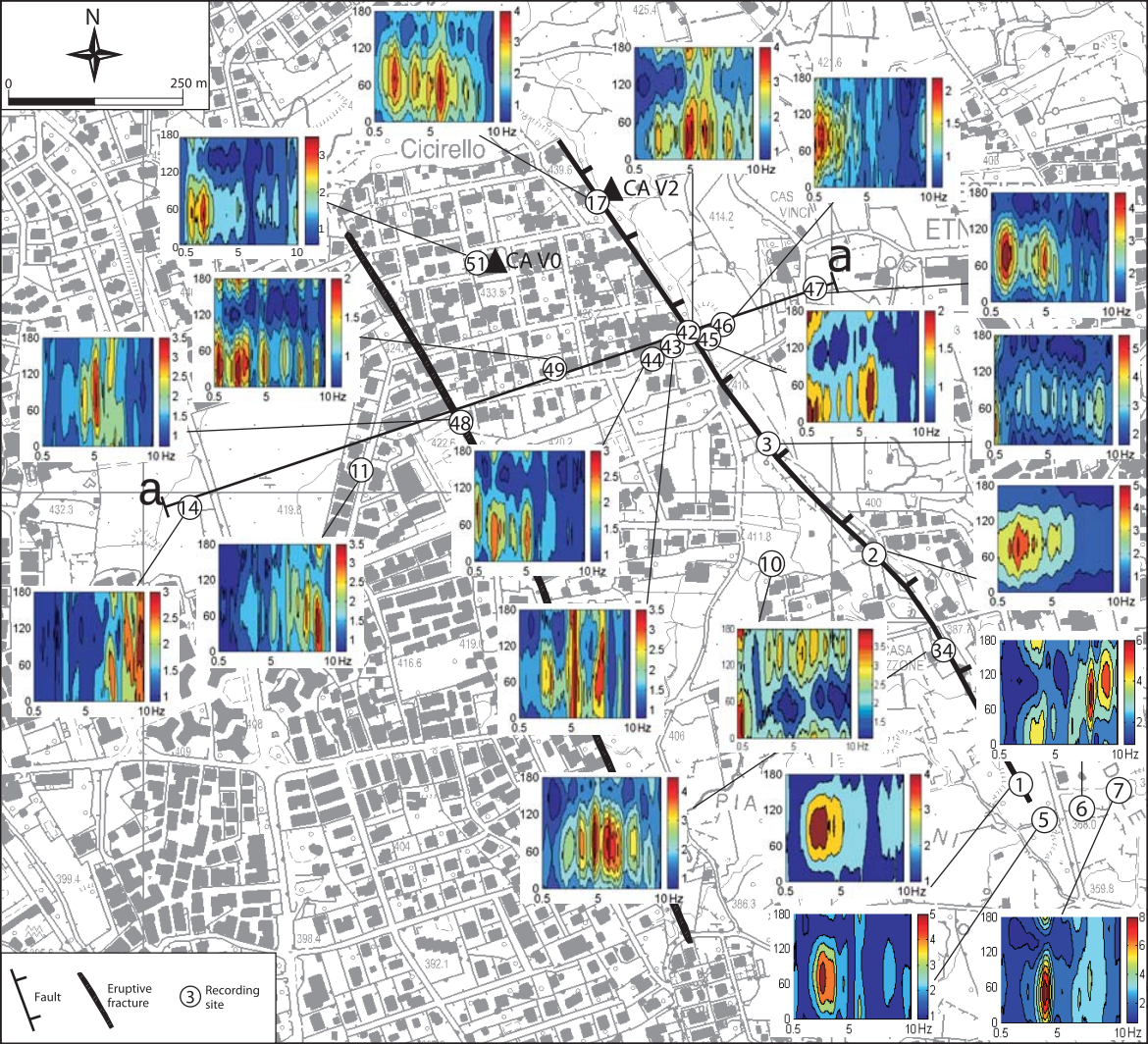
N
0
250 m
Cicirello
CA V2
CA V0
CAS VINCN
ETN
PIA
NI
ASA ZZONE
a
a
17
51
47
46
45
42
43
44
49
48
11
14
3
2
10
34
1
5
6
7
Fault
Eruptive fracture
3 Recording site

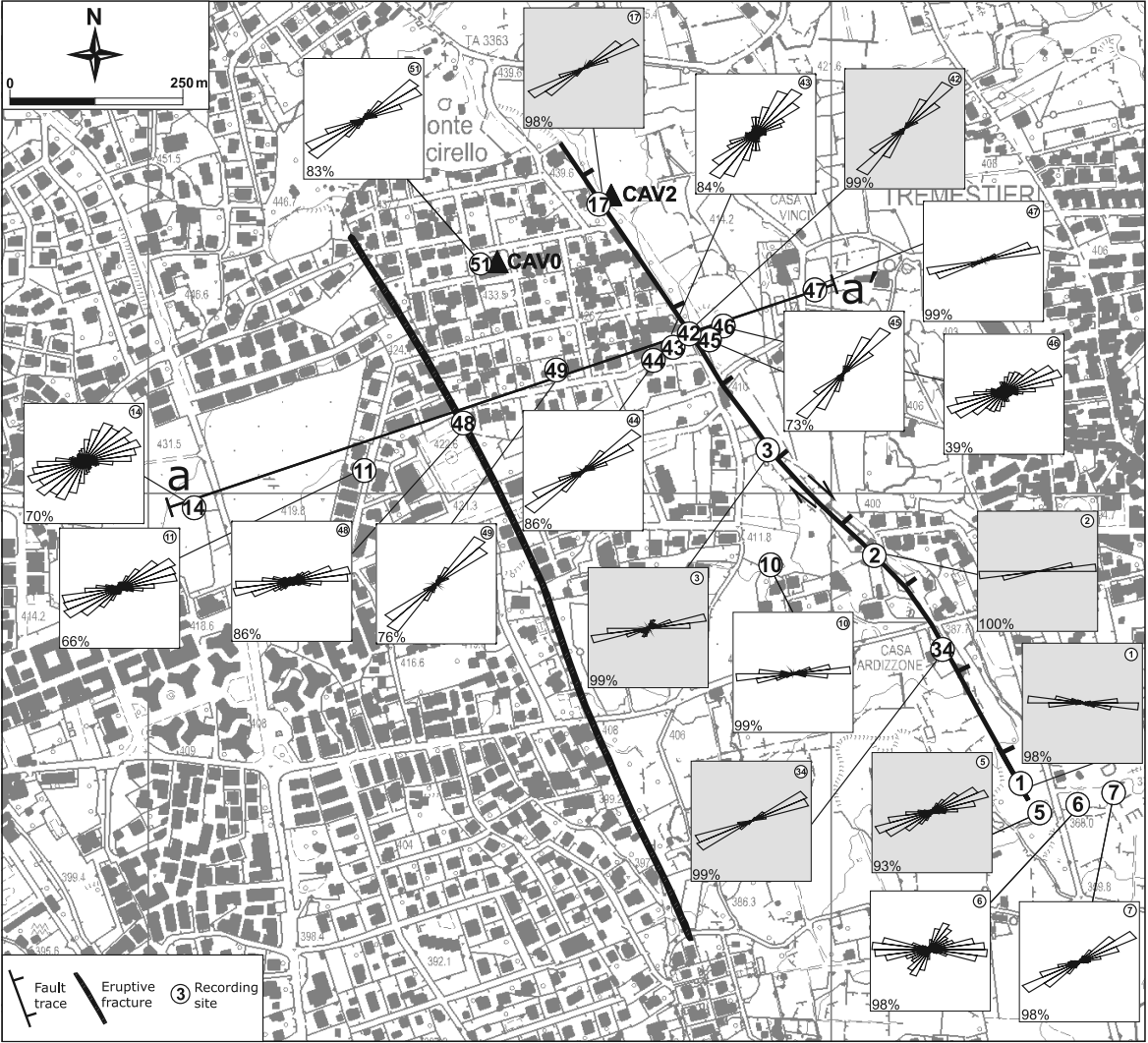
N
0
250 m
CAV2
CAV0
a
a'
TREMESTIER
CASA VINCI
CASA ARDIZZONE
Fault trace
Eruptive fracture
Recording site

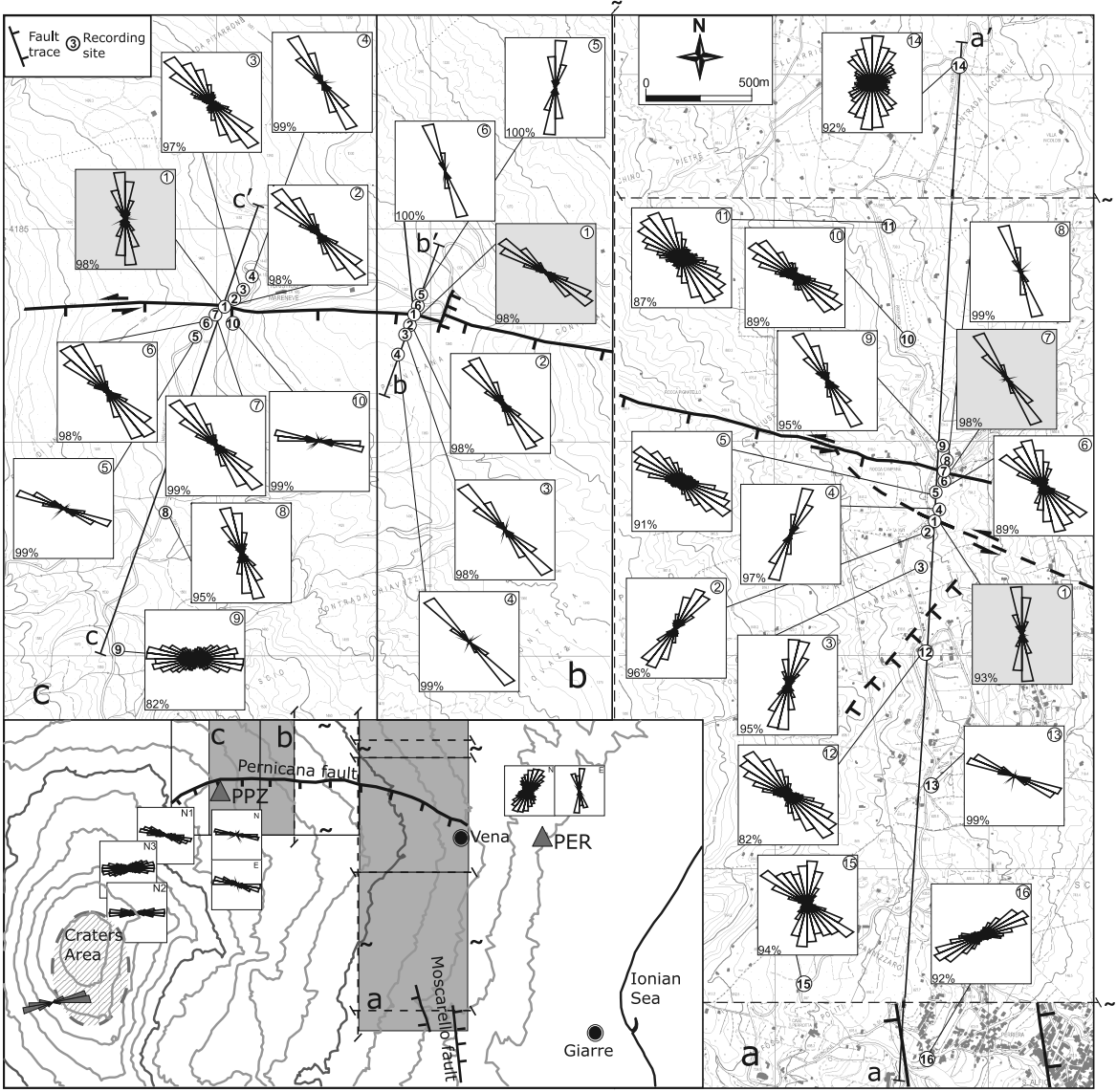
Fault trace
Recording site
N
0
500m
Pernicana fault
PPZ
Vena
PER
Crater's Area
Moscafello fault
Ionian Sea
Giarre
a
a'
b
b'
c
c'

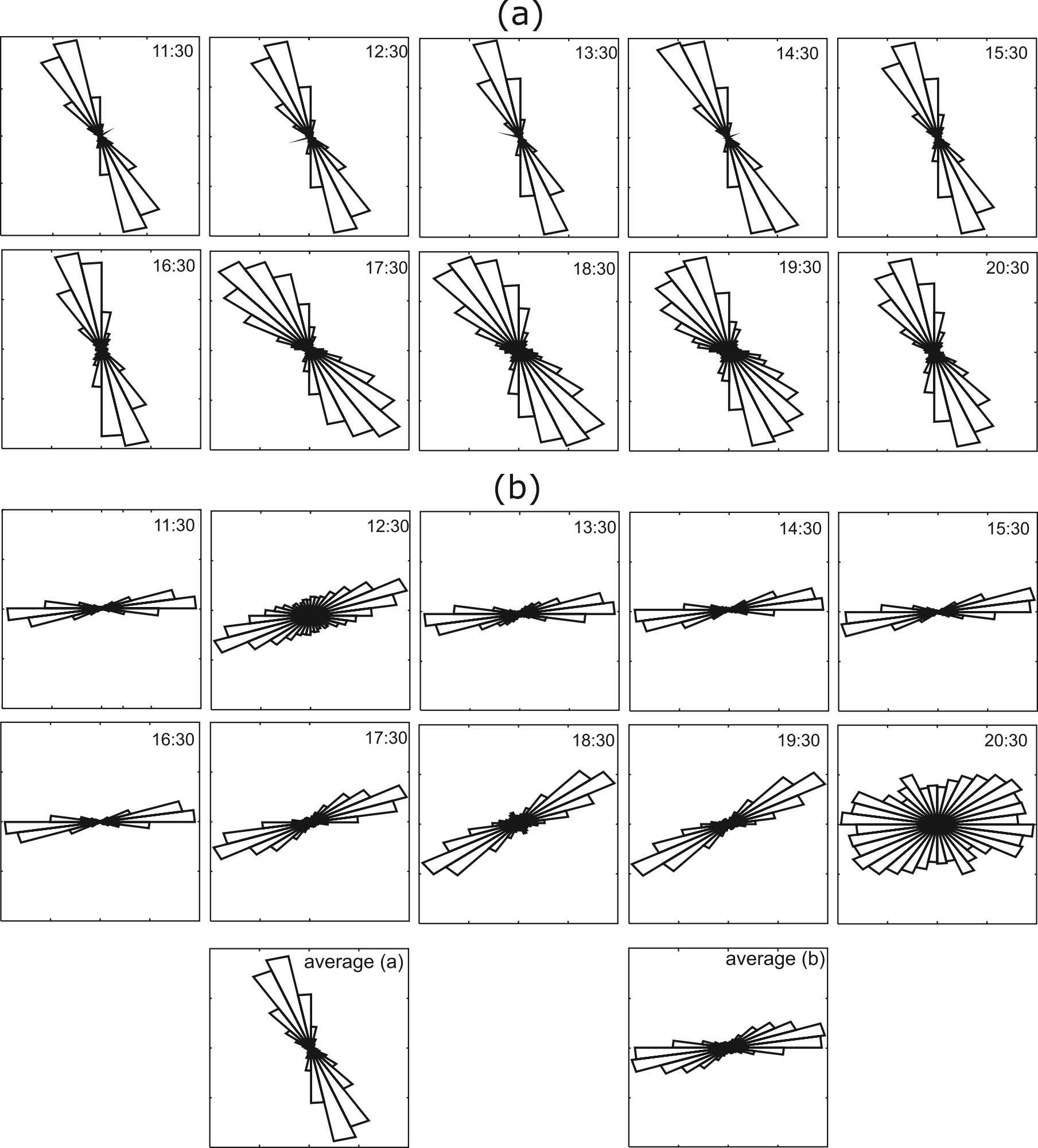
(a)
11:30
12:30
13:30
14:30
15:30
16:30
17:30
18:30
19:30
20:30
(b)
11:30
12:30
13:30
14:30
15:30
16:30
17:30
18:30
19:30
20:30
average (a)
average (b)

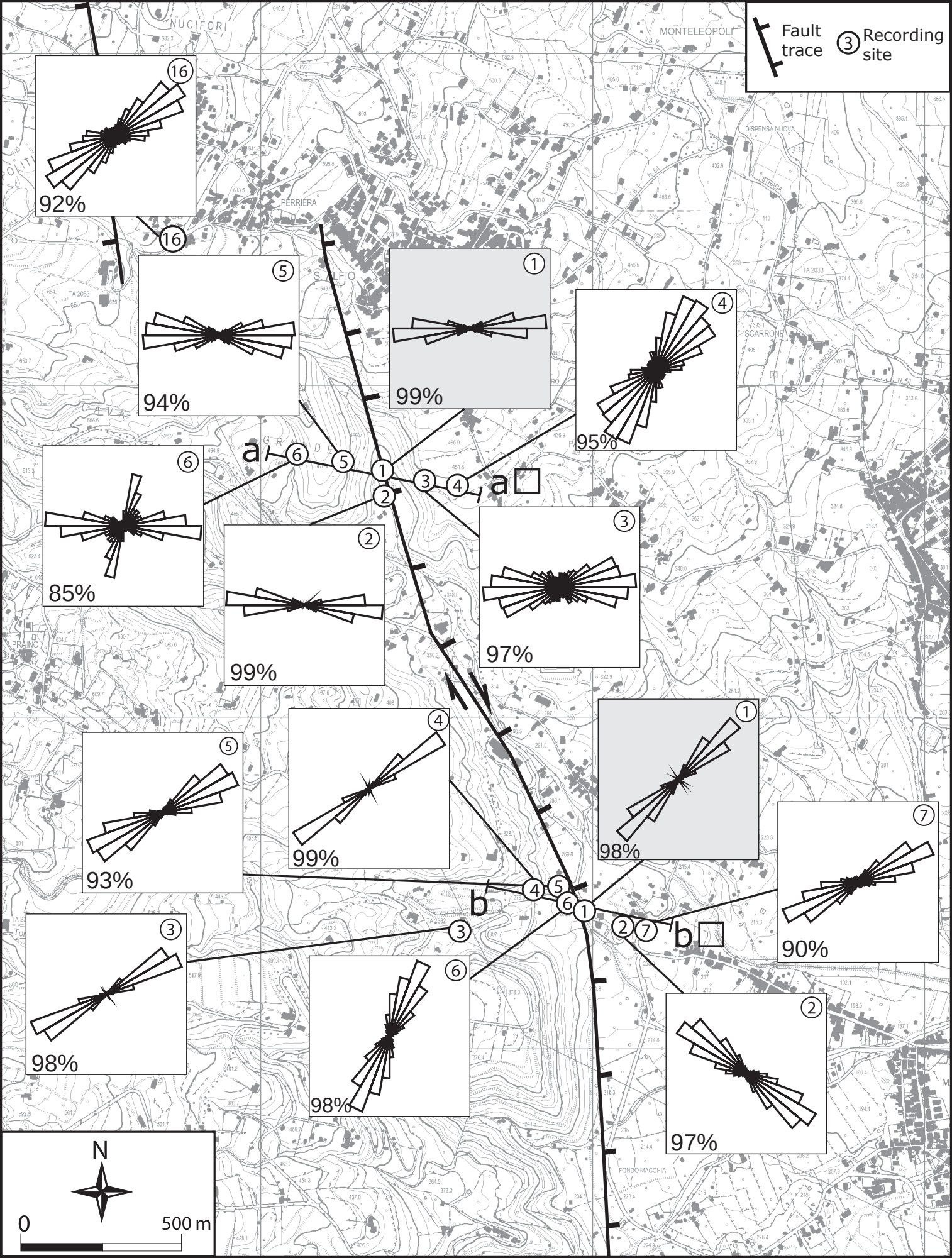
Fault trace
Recording site
92%
94%
99%
95%
85%
99%
97%
99%
93%
98%
90%
98%
98%
97%
a
a'
b
b'
N
0
500 m

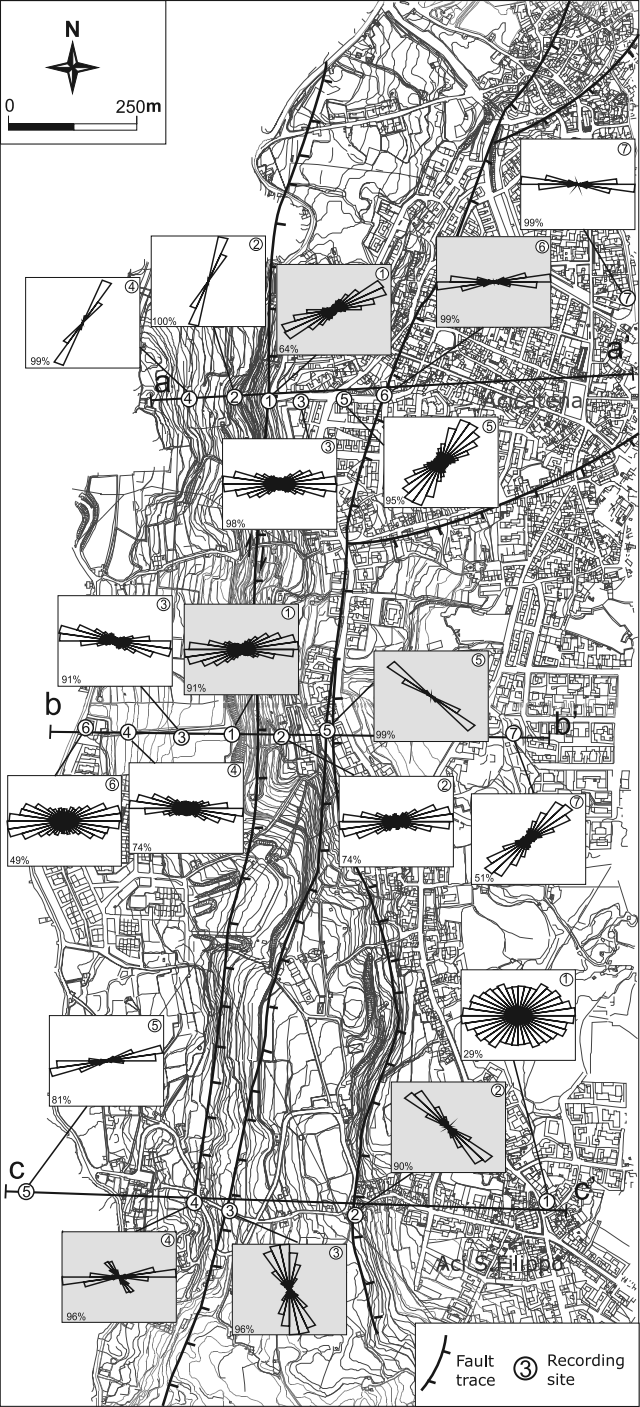
N
0
250m
a
a'
b
b'
c
c'
Acicastella
Acis S. Filippo
99%
100%
64%
99%
98%
95%
91%
91%
99%
49%
74%
74%
51%
29%
81%
90%
96%
96%
Fault trace
Recording site

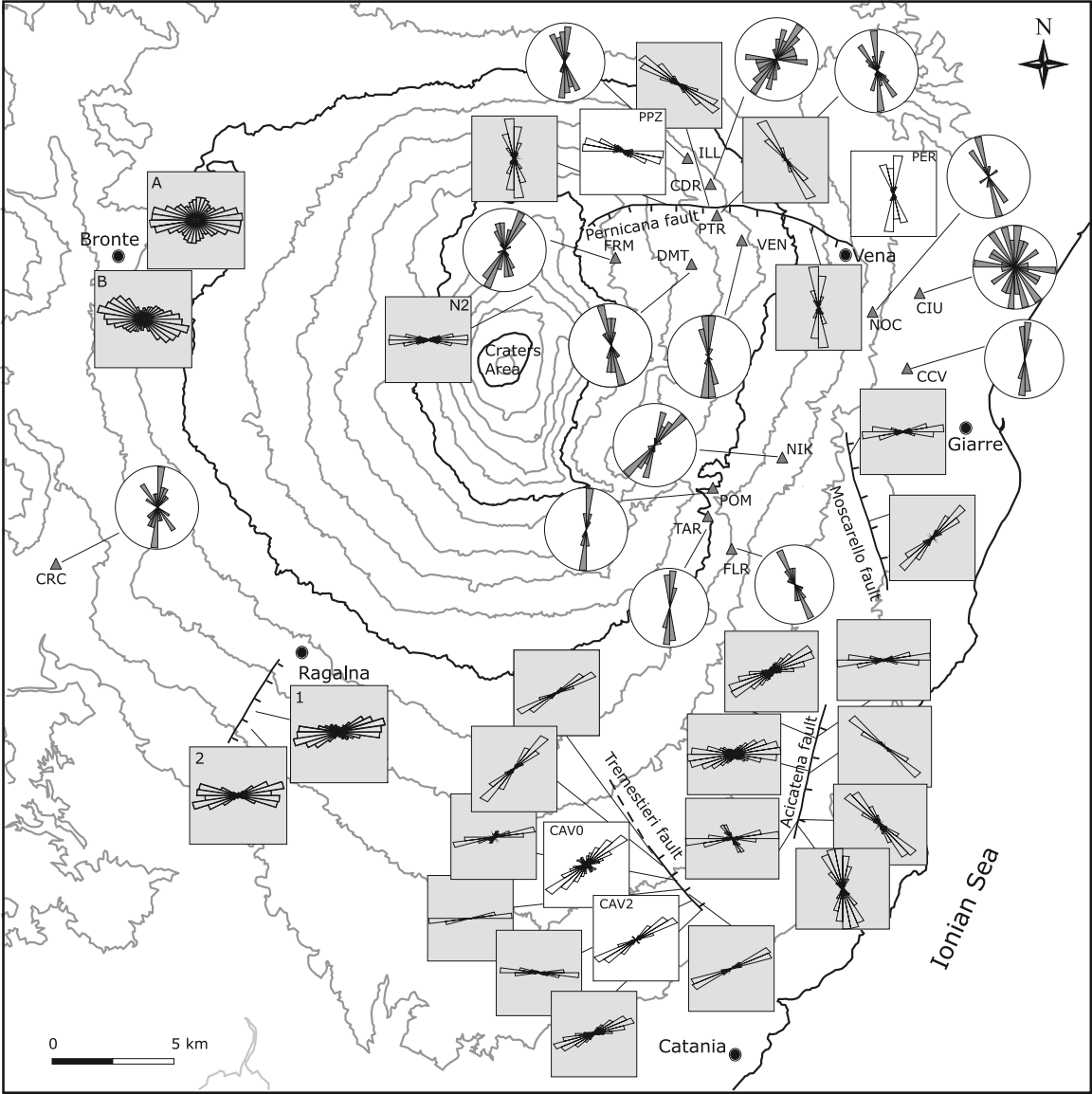
N
PPZ
ILL
CDR
PER
Pernicana fault
PTR
FRM
DMT
VEN
Vena
CIU
NOC
CCV
Giarre
Bronte
A
B
N2
Craters
Area
NIK
POM
TAR
FLR
Moscarello fault
CRC
Ragalna
1
2
Trecastagni fault
Acicatena fault
CAV0
CAV2
Ionian Sea
Catania
0
5 km